How the shape of fillers affects the barrier properties of polymer/ non-porous particles nanocomposites: A review

Caroline Wolf, Helene Angellier-Coussy, Nathalie Gontard, F. Doghieri, Valérie Guillard

How the shape of fillers affects the barrier properties of polymer/ non-porous particles nanocomposites: A review

C. Wolf, H. Angellier-Coussy, N. Gontard, F. Doghieri, V. Guillard

www.elsevier.com/locate/memsci

PII: S0376-7388(18)30097-8
DOI: https://doi.org/10.1016/j.memsci.2018.03.085
Reference: MEMSCI16079

To appear in: *Journal of Membrane Science*

Received date: 11 January 2018
Revised date: 29 March 2018
Accepted date: 30 March 2018

Cite this article as: C. Wolf, H. Angellier-Coussy, N. Gontard, F. Doghieri and V. Guillard, How the shape of fillers affects the barrier properties of polymer/ non-porous particles nanocomposites: A review, *Journal of Membrane Science,* https://doi.org/10.1016/j.memsci.2018.03.085

How the shape of fillers affects the barrier properties of polymer/ non-porous particles nanocomposites: A review

C. Wolf[1], H. Angellier-Coussy[1], N. Gontard[1], F. Doghieri[2], V. Guillard[1]

[1]UMR IATE, University of Montpellier, INRA, 2 place Pierre Viala, 34060 Montpellier Cedex 1, France

[2] DICAM University of Bologna, Via Terracini 28, I-40131 Bologna, Italy.

Abstract:

More than 1000 published experimental data of gas (O_2 and CO_2) and vapor (H_2O) permeability in nanocomposites containing either spherical, elongated or platelet particles were collected, assorted and compared in order to decipher the role of particle shape on the reduction of the relative permeability of the nanocomposite. It is well known that inclusion of homogeneously dispersed and oriented impermeable fillers with high aspect ratio, such as platelets or elongated particles, should significantly increase the diffusion path of gas and vapors and yield to improve barrier properties. Results revealed that this expected impact was not systematically achieved, even for impermeable lamellar fillers that usually displayed the highest aspect ratio. More specifically, an unexpected increase of the permeability in the nanocomposite was often observed. To explain this deviation of the 'ideal behavior', this paper discusses extensively the impact of the nanoparticle shape on the nanocomposite permeability along with structural aspects, related to both the particle nature and size, and the nanocomposite processing routes. Deviations from expected results of enhanced barrier effect are also discussed in correlation with unexpected variations in gas selectivity for O_2/CO_2 pair. Lastly, this review aims at drawing meaningful conclusions on the structure/mass transfer relationships and giving directions for the development of the next generation of packaging materials with tailored mass transfer properties.

Keywords:

Particle shape, Nanocomposites, Structure & mass transfer relationships, Permeability

1. Introduction

In the objective of developing efficient and optimal packaging, one of the main challenges is to design and provide food packaging materials able to protect the food from the external environment and to maintain food quality and safety throughout its shelf life [1,2]. The mass transfers are thus at the heart of the feature of the food packaging, especially transfers of water vapor, oxygen and/or carbon dioxide, which condition the rates of numerous reactions of food degradation (oxidation, microbial development, physiological reactions, etc.). The development of bulk nanocomposite structures by introducing nanoparticles, *i.e.* fillers having at least one dimension lower than 100 nm, in polymeric matrices appeared as one of the most promising directions in the development of packaging materials with advanced mass transfer properties. The expected role of these inclusions is to achieve a significant decrease of the mass transfer properties as compared to the neat matrix by acting as physical obstacles to the diffusion and permeation of diffusing molecules, which have to follow a more tortuous pathway. This phenomenon is called the tortuosity effect.

Many types of nanoparticles have already been tested to modulate mass transfer properties, with hundreds of permeability data published in literature. Nanoparticles can be classified into three major categories according to their particle shape (**Figure 1**): (i) *isodimensional particles,* that have the same size in all directions and an aspect ratio close to unity (such as spherical silica, TiO_2 nanoparticles, carbon black and fullerenes); (ii) *elongated particles* that consist in fibrils with a diameter ranging between 1 and 100 nm and length up to several hundred nanometers (such as carbon nanotubes or cellulose nanofibers); and (iii) *layered particles* that are characterized by one dimension ranging from several angstroms to several nanometers (such as layered silicates or starch nanocrystals).

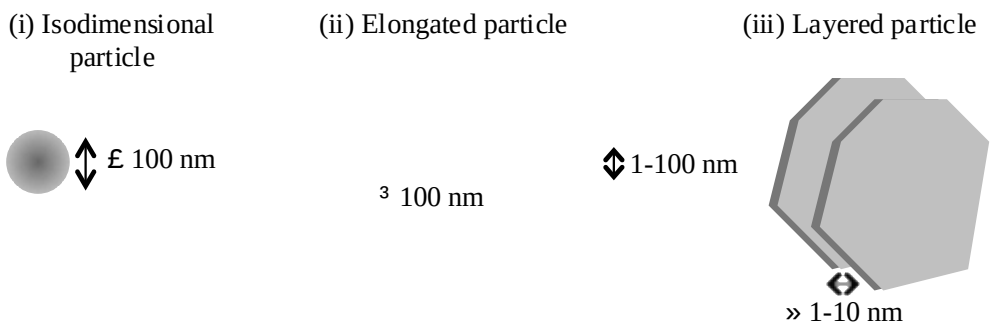

Figure 1. Schematic representation of the three categories of nanoparticles.

Among the three aforementioned types of particles, it is widely recognized that inclusion of impermeable platelets such as clays in the polymer should significantly enhance its barrier properties. However, an in-depth study of the available data in the literature revealed that it was not systematically the case and, even, on the contrary could lead to a deterioration of the barrier properties. Many reviews deal with the functional properties of nanocomposites, by mainly focusing on mechanical properties [3–14]. Among these studies, some of them focused slightly on the mass transfer properties [5,6,8–12] but without deepening the topic. These studies generally focused on one type of nanoparticle, *i.e.* spherical nanoparticles or nano-platelets for instance, particularly for membrane applications. Few of them focused on food packaging applications [13,15–18]. The last exhaustive review in the field is that of Cui et al. in 2015 [19] that focused on gas barrier properties of clay-based polymer nanocomposites. However, the effect of the platelet-shape has never been compared and discussed along with results obtained with spherical and elongated particle shape. In spite of all these preceding reviews, there is still a huge lack of analysis of all available data in the perspective of deciphering the role of particle shape on the mass transfer properties of the resulting nanocomposite materials, even if it has been highlighted as a key input parameter in mathematical models. As far as we knew, there is no review that proposes an exhaustive analysis of the experimental permeability values from the available literature.

In order to better correlate the mass transfer properties in nanocomposite materials with their multi-scale structure, the objective of the present review is to decipher and comprehensively discuss the role of the nanoparticle shape (either isodimensional, elongated or layered) on the modulation of the mass transfer properties in nanocomposites, as a function of filler volume fraction and in the light of the nanocomposite structure achieved. For that purpose, more than 1000 values (i.e. about 170 articles) of the 1995-2015 period containing measured values of O_2, CO_2 and H_2O permeability in polymer-based nanocomposites were collected from the available literature and capitalized in a dedicated on-line database [20]. All data could be uploaded from the permalink provided in figure caption (https://doi.org/10.5281/zenodo.1136269). The proposed on-line database consists in the first and unprecedented compilation of permeability values

for nanocomposite based materials. The current work is focused on direct analysis and comparison of experiments, without any mediation which could be provided by quantitative models. It must be specified that, in order to build up the database for analysis, which is of interest here, recent data for gas barrier in polymer based materials with dispersed graphene and graphene derivatives were not taken into consideration. In fact, while the latter represent nanocomposite materials with dispersed layered domains, the extremely high aspect ratio and flexibility of graphene layers reduces the threshold value for percolation in these materials to much lower values than in traditional layered particles nanocomposites [21]. Under those conditions, in the volume concentration range for layered particles which is of reference in this work (in the order of 10% by volume) layers arrangement and layer defects are significantly more relevant to the barrier effect than the aspect ratio (particle shape) itself. For a comparison between gas barrier properties in polymer/clay and polymer/graphene nanocomposite see the review by Tan [22]. For the above reason, although graphene has attracted much attention in recent years, here also for the production of polymer based composites for packaging [] analysis of pertinent results for gas barrier properties is left to a different discussion and the interested reader is addressed to recent reviews in the field [23].

Besides the meaningful conclusions on the role of nanoparticle shape, the main output of this paper is to give some recommendations for the design of nanocomposite packaging materials with tunable mass transfer properties.

2. Brief overview of nanocomposites processing and morphologies

All the processes used to prepare polymer-based nanocomposites have already been extensively detailed in dedicated reviews and are not further detailed here. Examples of reference publications for layered silicates-based nanocomposites are those of Alexandre & Dubois [4], Ray et al. [11], Pavlidou et al. [6], Mittal et al. [9] and Cui et al. [19], for natural fiber-based nanocomposites, those of Saheb et al. [24] and Siqueira et al. [25] and for inorganic spherical particle-based nanocomposites, those of Cong et al. [8] and Chung et al. [5]. Due to the large range of polymer matrices and nanoparticles, different processing routes have been proposed to produce nanocomposites based on their convenience according to the nature of

the raw constituents and their field of application (**Figure 2**). At laboratory scale, four main processes are most commonly used to prepare polymer-based nanocomposites from all the types of nanoparticles. Melt processing and solution blending are two processes based on the use of polymers, which lead to the formation of Van der Waals interactions between the constituents, while in-situ polymerization and sol/gel methods are based on the use of monomers or oligomers, leading to the formation of covalent bonds between the polymer and the nanoparticles (Figure 2). At industrial scale, melt processing is generally preferred due to the difficulty to implement processes requiring the use of huge volumes of solvent.

Depending on the processing conditions, the particle shape and the affinity between constituents, *i.e.* the polymer matrix and the nanoparticle, different morphologies can be obtained. For isodimensional and elongated nanoparticles, three arrangements can be observed, *i.e.* (i) well-dispersed, (ii) agglomerated, or (iii) percolating systems. For platelets, specific names are given to the various possible morphologies: (i) micro-composite, (ii) intercalated nanocomposite or (iii) fully exfoliated nanocomposites. The micro composite structure corresponds to the formation of tactoïds and appears when the polymer chains do not manage to penetrate into the layered sheets due to, mainly, a poor particle/polymer matrix affinity, an insufficient interlayer distance and/or an inefficient shearing during the process. Intercalated nanocomposite structures are obtained when the polymer chains have diffused between silicate layers, leading to an increase of the interlayer distance. Exfoliated nanocomposite structures are characterized by a complete delamination and homogeneous dispersion of the layered sheets. Depending on the process, an isotropic (random) or anisotropic orientation could be achieved (for example platelets orthogonal to the diffusion flux).

A good knowledge of the morphologies obtained is an indispensable prerequisite to well understand variations of mass transfer properties in the nanocomposite materials.

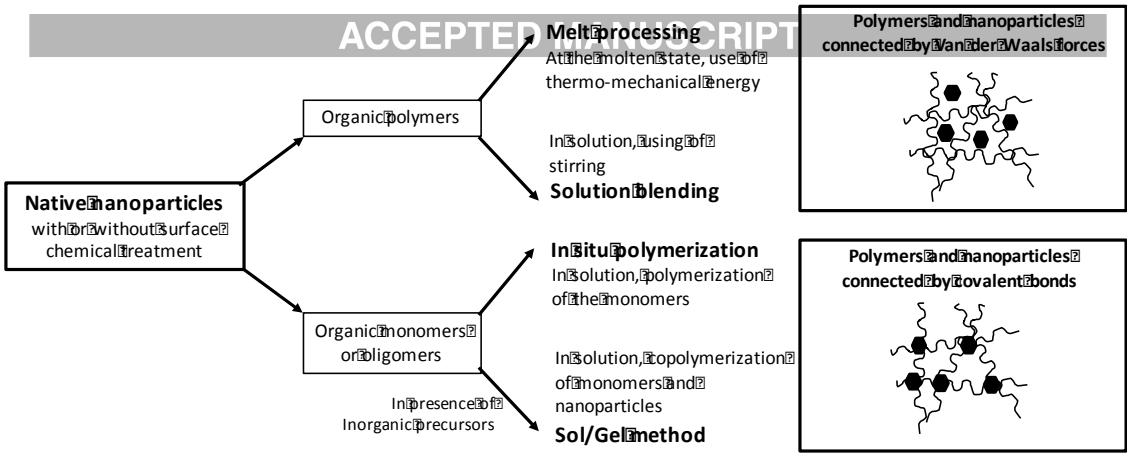

Figure 2: Outline of the preparation techniques of nanocomposite based materials

3. Effect of the nanoparticle shape on the modulation of mass transfer properties

3.1. Theoretical background

A great amount of effort has been made in the literature to describe the effect on transport properties of the inclusion of non-conducting particles into a conductive matrix and the effect of particle shape has been a focus since the beginning of these studies. Similar analyses of the problem can be found in the field of electrical properties (electrical conductivity/permittivity) as well as in that of heat or mass transfer (thermal conductivity /mass diffusivity). Exact solutions in terms of effective conductivity of the composite medium have been obtained already by Maxwell in 1873 [26] for the case of dilute mixture of spherical domains ("non-interacting particles") perfectly adhering to the matrix. These exact solutions assume that the properties of dispersed and continuous phase in the composite are the same than the one measured in the corresponding pure materials ("ideal interface condition").

Wiener [27] in 1912 extended the results to the case of dilute dispersion of long cylinders in the matrix, all aligned in the direction normal to the overall flux. While exact solutions are also available for the case of spheroids (dilute mixture, perfect alignment), empirical relations as well as numerical result have been discussed for the case of different shapes of the inclusions. Among the best, known results of this kind are those obtained by Nielsen [28] in 1967 following empirical ideas about the increase in contour length of

path of diffusing molecules in the composite medium due to the presence of impermeable inclusions in the form of bricks. The specific expression for effective conductivity as function of particle concentration in the composite as derived from the above models is not here presented and discussed, as the direct comparison of available experimental results with model predictions is not in relevant to this work. On the other hand, it is useful to remember here that all the above approaches consistently predict a decrease in the conductivity when the concentration of impermeable particles in the composite increases. In general terms, it can be said that, assuming ideal interface and non-interacting particle condition, the effective conductivity of the composite medium is expected to be half the value of the pure matrix when the concentration of dispersed phase approaches 40% vol for isometric particles, 30% vol for elongated particles aligned normally to the flux, and a much lower value, only few percent, depending on the exact shape, for layered particles lying in planes orthogonal to the flux.

It should be finally mentioned that more complex analyses are definitely needed to consider the interaction between particles in the medium (concentrated mixtures), the distribution in their orientation, as well the non-ideal interaction with the matrix which can ultimately result in regions close to the interface with properties different from that of pure materials [29].

3.2. Explanation of the analysis approach

The publications considered in the following part were collected from peer-reviewed scientific journals published between 1995 and 2015 in different fields of research such as membrane, materials and packaging sciences. All these papers, dealing with nanocomposite materials, presented at least one value of permeability in relation to their composition. The nanoparticles considered in works examined in this review are those assumed as impermeable and non-porous with respect to the application that is focused on: barrier membranes mainly for packaging application. Moreover, it must be noted that mass transfer does not follow the same mechanisms in dense and porous material and that mixing porous and non-porous materials may disturb the analysis. Only gases (O_2 and CO_2) and water vapor permeability data were considered because of their high interest for food packaging applications. These data were analyzed as regard to the particle shape (isodimensional, elongated, or platelet), the filler volume fraction, the eventual

chemical and functionalization treatments applied to the nanoparticle and the elaboration technique used to prepare materials. The main characteristics of the nanocomposites studied in the present review are gathered in **Tables 1, 2 & 3**.

Tables 1, 2 and 3 (*these tables are provided at the end of the manuscript for the sake of clarity***)**

In the following, the evolution of the relative permeability, *i.e.* the ratio of the composite permeability to the permeability of the neat matrix (P/P_0), was represented as a function of the nanoparticle volume fraction (ϕ_{vol}), which is considered as input parameter in all mathematical models. This implied to systematically calculate ϕ_{vol} values from weight fractions (ϕ_{wt}) values given in the original papers, based on the knowledge of the true density of each constituent (equation 1):

$$\phi_{vol} = \frac{\frac{\phi_{wt}}{\rho_{nanoparticle}}}{\frac{\phi_{wt}}{\rho_{nanoparticle}} + \frac{1-\phi_{wt}}{\rho_{matrix}}} \quad \textbf{[1]}$$

where ρ_{matrix} and $\rho_{nanoparticle}$ are the true density of the matrix and the nanoparticles respectively. Such a conversion led to unavoidable uncertainty on ϕ_{vol}.

3.3. Modulation of mass transfer properties in nanocomposites: global evolution of P/P_0

Most of the studies of O_2, CO_2 and H_2O permeability in nanocomposites were carried out in platelets-based nanocomposites with about 100 publications on the topic resulting in a total of 710 permeability values. All of them have been represented in **Figure 3c** leading to a scatter graph in which each individual study could not, of course, be distinguished. For comparison, 45 publications were found for isodimensional nanoparticles-based nanocomposites against 22 for elongated nanoparticles-based nanocomposites, resulting in about 380 and 120 permeability values respectively (**Figures 3a** and **3b**). Papers dealing with elongated particle displaying micrometric sizes (13 papers more) were voluntary excluded from this review. Due to the high number of studies found for each type of particle shape (for O_2, CO_2 and H_2O permeability), the figures are overloaded and thus not easily readable. Three complementary figures have been drawn for each type of particle shape and for each molecule studied, i.e. O_2, H_2O and CO_2 respectively. Analysis of these general figures permits to highlight the intensive work on the topic and to draw the general

tendencies of P/P_0 variation as a function of nanoparticle shape and ϕ_{vol} and nature of the penetrant. The following observations can be made:

- The investigated ϕ_{vol} range is higher for isodimensional and elongated nanoparticles than for platelets with maximal ϕ_{vol} values of 40 vol% and 45 vol% respectively (Figures **3a** and **3b**), against 15 vol% for nanoplatelets (Figure **3c**). Only 3 publications (*i.e.* 11 permeability values) were in the range of 15-40 vol% for nanoplatelets-based nanocomposites (not shown in Figure **3c**). This feature could be ascribed to the fact that usually, only a small weight fraction of nanoplatelets (generally 1 to 5 wt%) is necessary to obtain a significant effect on the material functional properties.

- The evolution and variation amplitude of P/P_0 as a function of the nanoparticle volume fraction is really complex and does not follow the same trend according to the shape of nanoparticles (**Figure 3**). Figures **3a** and **3b** permit to point out that the addition of isodimensional or elongated nanoparticles in a polymer generally provokes either a monotonic decrease or increase of P/P_0 with an amplitude of variation ranging from 0.15 to 16 and from 0.1 to 18, respectively. This leads to a scatter graph of P/P_0 with a general aspect in herringbones centered on P/P_0 =1. On the contrary, Figure **3c** shows that for nanoplatelets, except for one or two cases, P/P_0 values remain always below 1.

- The maximum drop in P/P_0 is much higher for nanoplatelets-based nanocomposites, with P/P_0 reaching a minimum value of 0.01, *i.e.* up to 10 folds lower than the minimum value reached with elongated nanoparticles, and in spite of the lower filler volume fractions used.

- For all the kinds of nanoparticles, some non-monotonic variations of P/P_0 are noted with simultaneous increase and decrease of the relative permeability for the nanocomposites. It represents approximately 12% of the studies for isodimensional nanoparticles, 21% of the study for elongated nanoparticles and only 7% of the studies for nanoplatelets.

- Analysis of the trends per type of penetrant, O_2, H_2O and CO_2 respectively, did not lead to find some difference on P/P_0 regarding the molecules studied related to geometry. We also noted that the nature of the material depending of particle geometry did not influence the trends observed on the general figure.

Among the aforementioned conclusions of this first general analysis of P/P_0 evolution, some trends were expected, including the fact that nanoplatelets generate, more often and with a higher amplitude than elongated and/or isodimensional nanoparticles, a decrease of the permeability. This could be easily ascribed to the particle geometry and the more pronounced tortuosity effect induced by platelets as compared to spheres or cylinders. To go further, an in-depth, quantitative analysis of the data collected and capitalized was carried out.

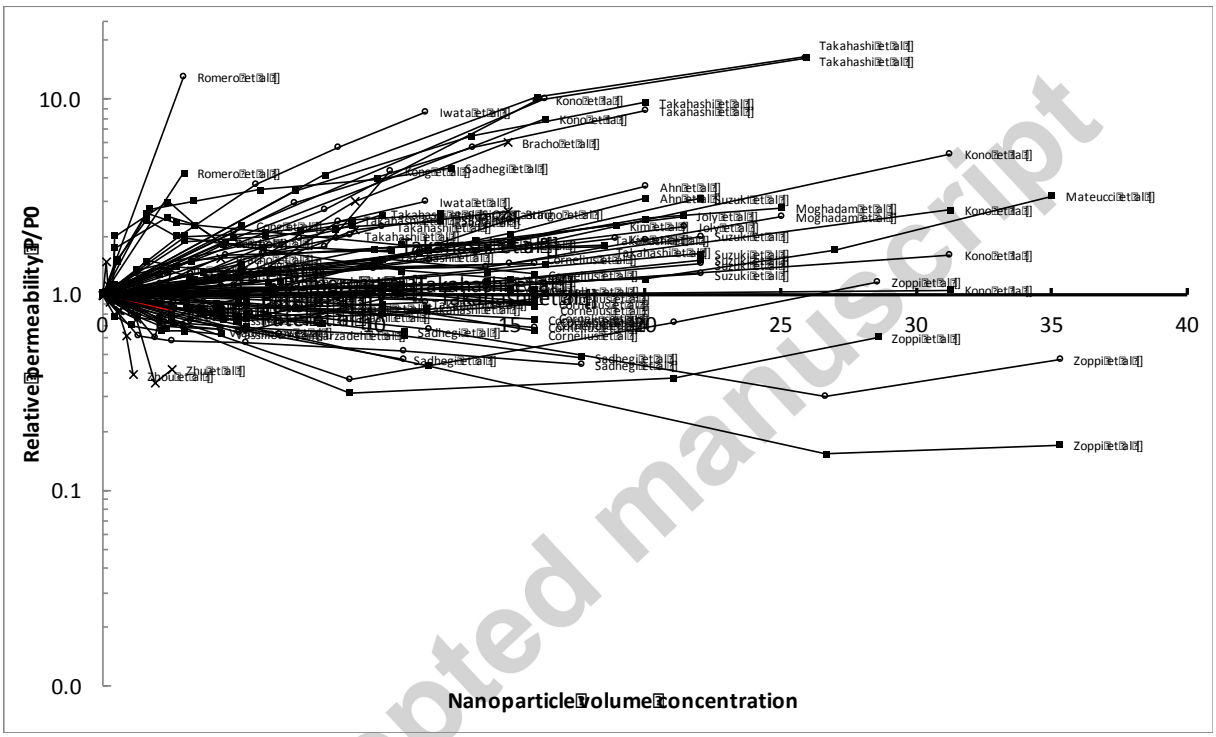

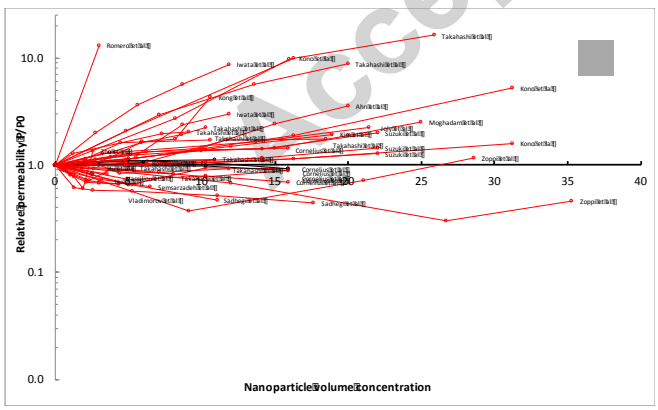

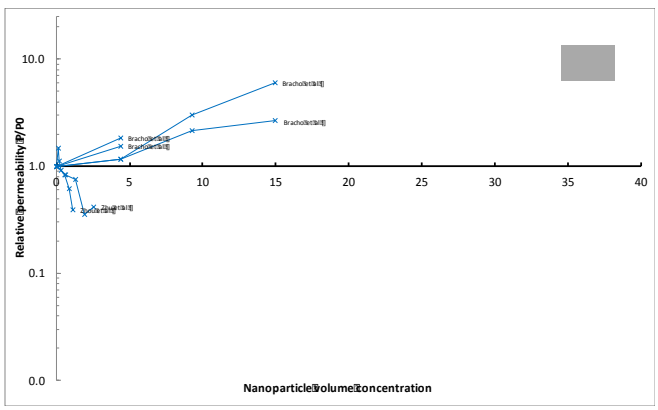

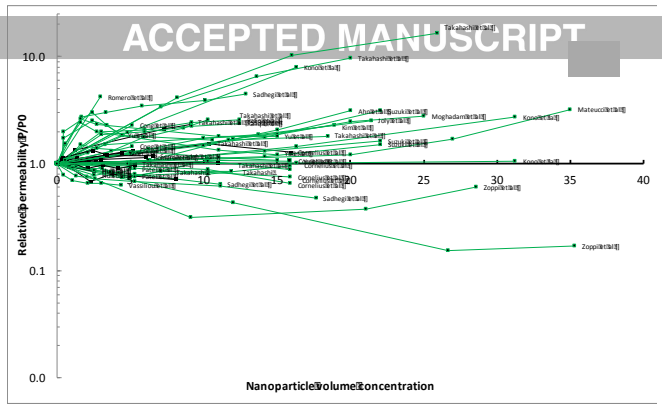

a. Isodimensional particles

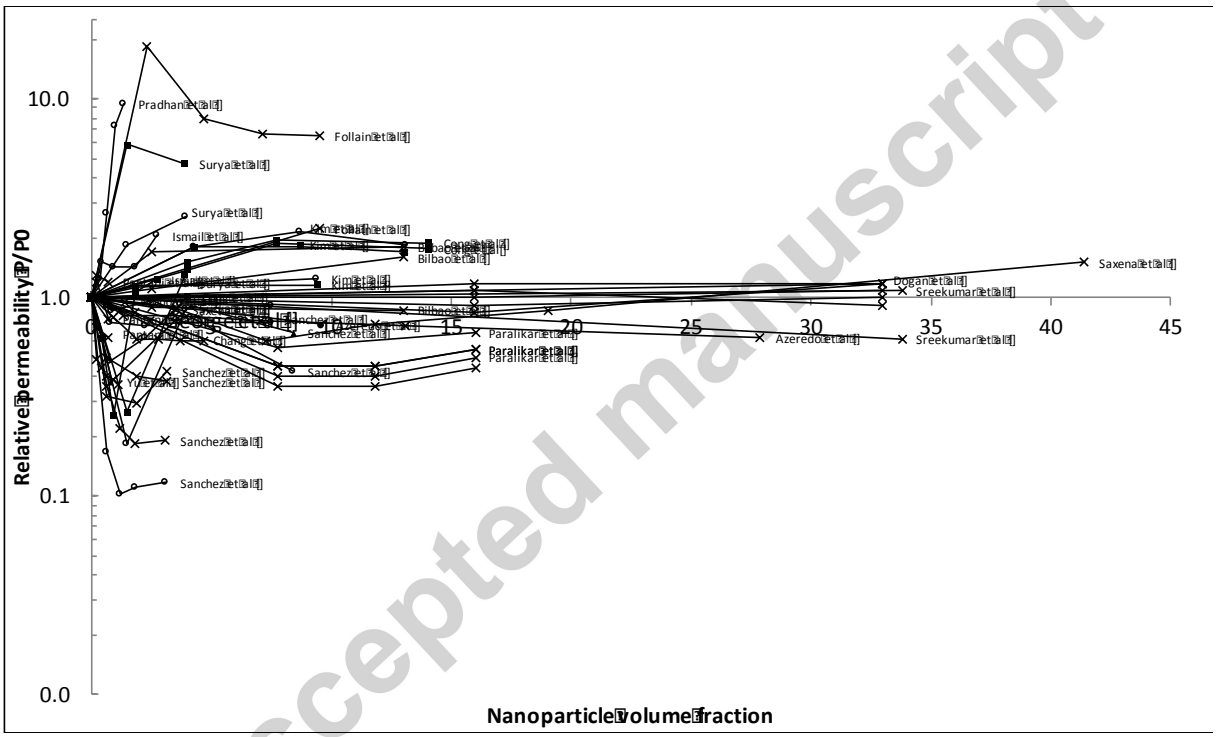

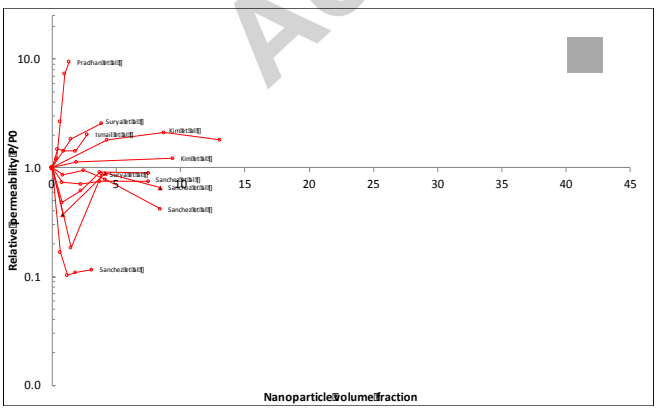

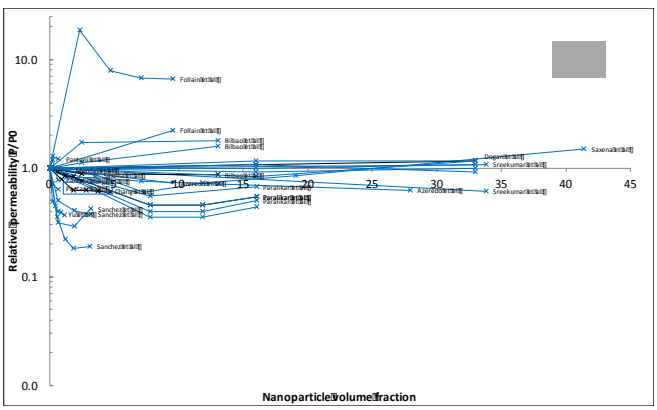

Comment citer ce document :
Wolf, C., Angellier-Coussy, H., Gontard, N., Doghieri, F., Guillard, V. (2018). How the shape of fillers affects the barrier properties of polymer/ non-porous particles nanocomposites: A review. Journal of Membrane Science, 556, 393-418. , DOI : 10.1016/j.memsci.2018.03.085

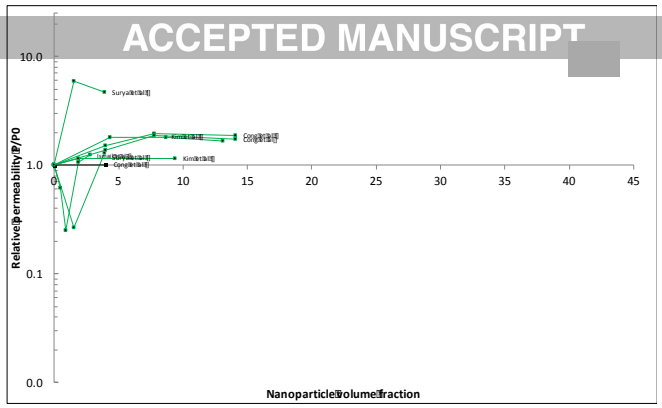

b. Elongated particles

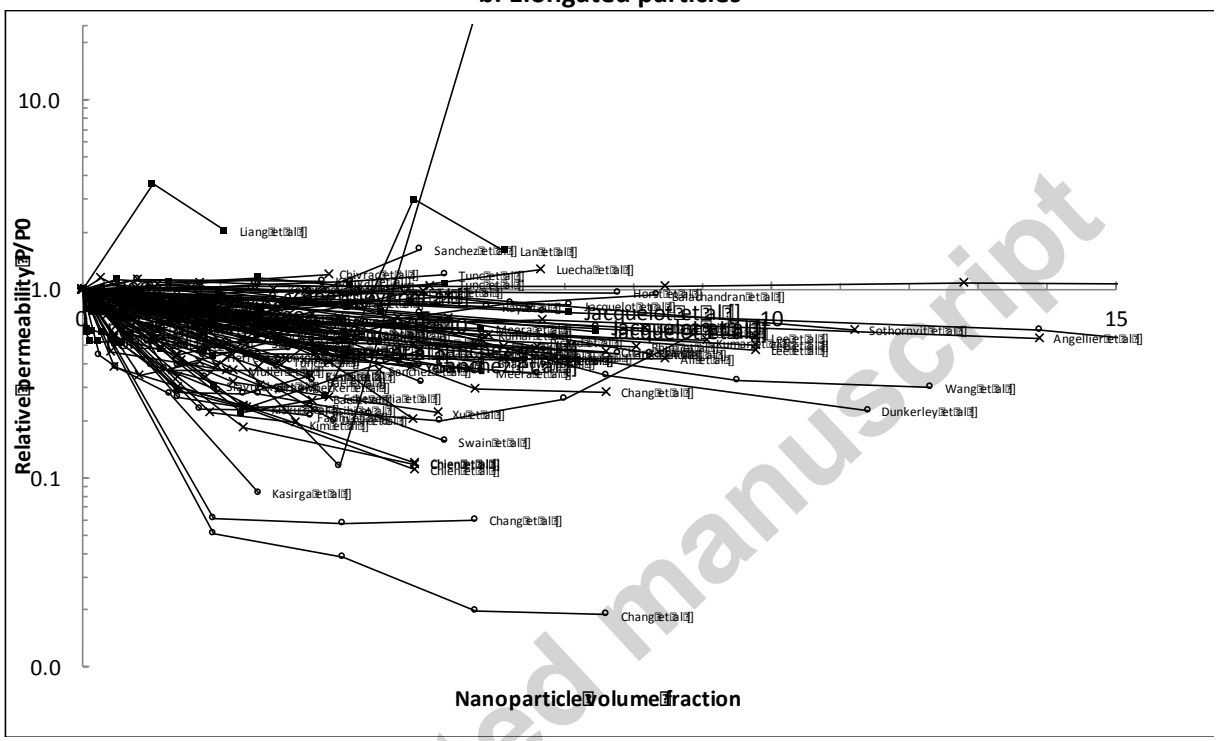

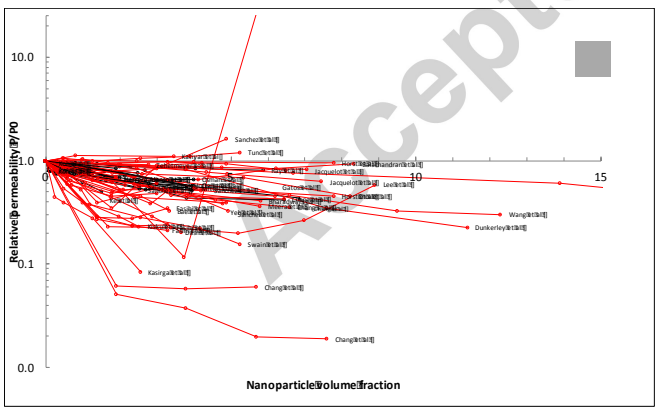

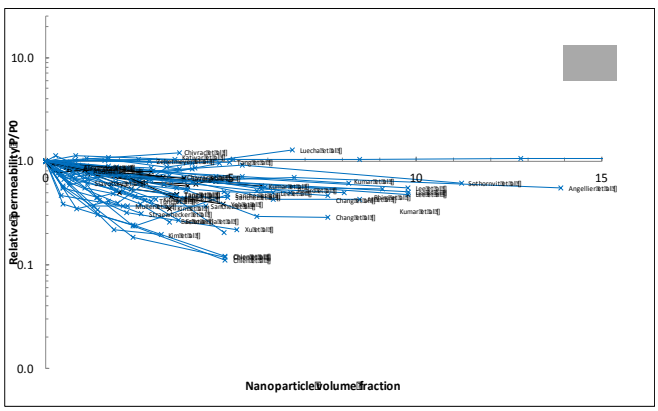

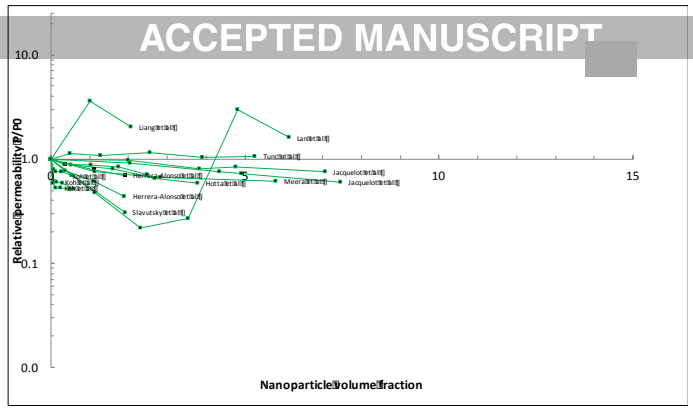

c. Layered particles

Figure 3: Evolution of the relative permeability P/P_0 as a function of particle volume fraction in nanocomposite material containing either (a) iso-dimensional, (b) elongated or (c) layered particles. From references listed in Tables 1, 2 and 3 respectively. Raw data can be uploaded from https://doi.org/10.5281/zenodo.1136269.

3.4. In-depth analysis of the modulation of mass transfer properties per type of nanoparticle

In order to perform a quantitative analysis of the efficiency of each type of nanoparticle shape on P/P_0, all the permeability data collected in the literature were gathered on a histogram displaying the percentage of values per class of modulation, *i.e.* per range of P/P_0 values. The maximum number of permeability values collected for isodimensional (43%), elongated (29%) and layered (30%) nanoparticles is obtained for the classes $1 < P/P_0 < 2$, $1 < P/P_0 < 2$, and $0.6 < P/P_0 < 0.8$ respectively, confirming that layered nanoparticles were more prone to improve the barrier properties of a given polymer (**Figure 4**).

Besides this main impact, secondary peaks are observed on **Figure 4**. In the case of isodimensional nanoparticles, 17% of values are obtained for the class $2 < P/P_0 < 3$ and 14% for $0.8 < P/P_0 < 1$, indicating that the permeability in these nanocomposites could be equally multiplied by a factor of 3 or slightly decreased by a factor of 0.8. This feature confirms well the herringbone scatter graph observed when all P/P_0 data are plotted as a function of ϕ_{vol} (**Figure 3a**).

In the case of elongated nanoparticles, 17% of collected data belong to the class $0.6 < P/P_0 < 0.8$ and another 17% to the class $0.8 < P/P_0 < 1$. This indicated that even if the main observed effect of the addition of elongated nanoparticles is a weak increase of permeability up to a factor 2, it could also statistically lead to a decrease of the permeability.

In the case of layered nanoparticles, the overall trend of decreasing permeability is confirmed by the occurrence of secondary peaks, which reveals that 23% of permeability values were obtained for $0.4 < P/P_0$ 0.6 and 21% for $0.8 < P/P_0 < 1$. In all the cases, P/P_0 values higher than 3 are very rare (less than 6% of the studies for every particle shape).

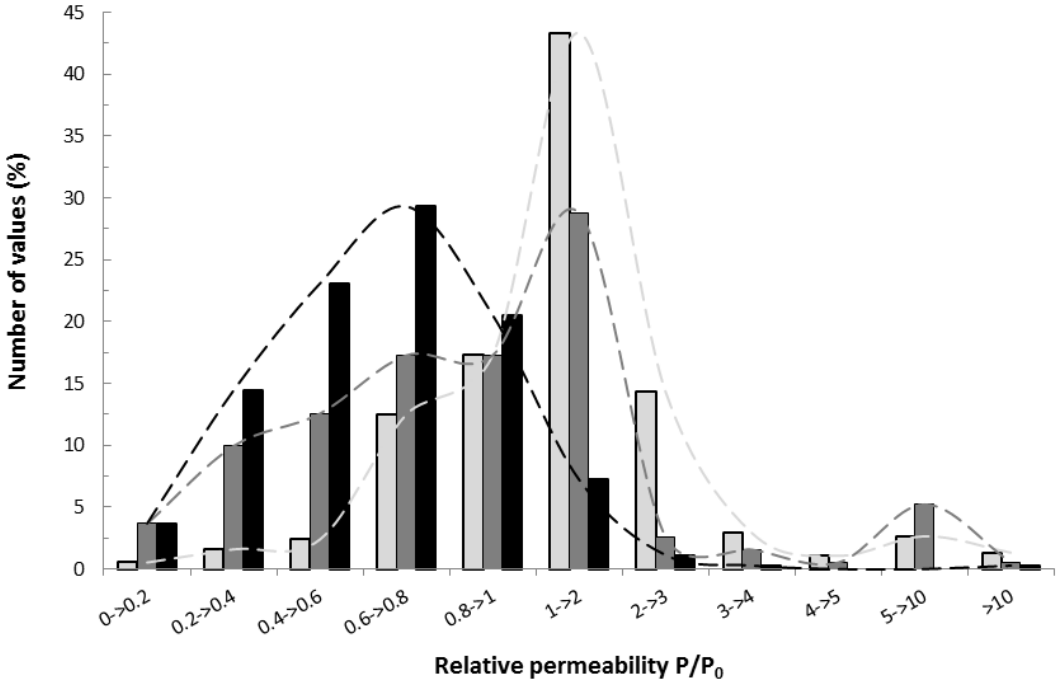

Figure 4. Percentage of permeability values collected in literature for nanocomposites filled with either iso-dimensional/spherical (light-grey), elongated (dark-grey) or layered (black) nanoparticles as a function of the classes of the relative permeability P/P0

To verify if the conclusions drawn from this global analysis were confirmed for all the tested filler contents, permeability values were also apportioned into classes of filler volume fraction in addition to the classes of P/P_0 values (**Figure 5**). The classes chosen for filler fractions were 0-5 vol%, 5-10 vol%, 10-20 vol% and 20-30 vol%. For this analysis, the range for P/P_0 was limited to a maximal value of 3, considering that a higher increase of the permeability ratio was an exceptional behavior. In the case of isodimensional nanoparticles, exactly the same evolution of P/P_0 is obtained for each filler fraction, with an increase up to a factor 2 of the permeability in almost 45 % of the cases (**Figure 5a**). For elongated nanoparticles, the same increase of P/P_0 is obtained but only for filler contents lower than 20 vol%. For higher filler contents, no clear tendency is evidenced, with a disordered shape of the curve. This could be due to agglomerated or percolated structures that become frequent for such high concentration in fillers whose effect

on permeability is more unpredictable (**Figure 5b**). Finally, for nanoplatelets-based nanocomposites, for filler contents lower than 5 vol%, the evolution of P/P_0 is the same as the general one previously observed on **Figure 4** and is characterized by a main peak (30% of data) centered on the class 0.6 to 0.8. This main peak shifts to lower P/P_0 values, *i.e*. better efficiency, for filler contents ranging from 5 to 10 vol%, with a main peak (38%) for P/P_0 values in the range of 0.4 to 0.6. For filler content higher than 10 vol%, the decrease in permeability is not confirmed anymore. We noted that studies conducted with such high amounts of platelets (> 10 vol%) were scarce, which makes it difficult to generalize the effect of high contents of platelets on the permeability of resulting nanocomposites (**Figure 5c**).

To sum up, beyond the fact that modulation of the permeability is clearly affected by the shape of the nanoparticles, three conclusions remain:

(i) whatever the filler content, the addition of isodimensional particles does not statistically impact the permeability of resulting nanocomposites very much,

(ii) a significant decrease of permeability could be achieved by nanostructuring polymer matrices with the introduction of either elongated or nanoplatelets-shaped nanoparticles, with a much higher efficiency of layered nanoparticles. Indeed, the use of filler contents higher than 20 vol% are necessary to achieve a significant decrease of P/P_0 in the case of elongated nanoparticles while less than 10 vol% are sufficient in the case of nanoplatelets,

(iii) the barrier effect of nanoplatelets is even more pronounced for filler contents ranging from 5 to 10 vol%.

This analysis has also revealed that the behavior of P/P_0 is more complex than expected, with the occurrence of non-monotonic behaviors, especially in the case of elongated nanoparticles. In the following, lines of explanation will be tentatively brought in order to relate this “shape effect” to the morphology of the particle and the (nano)-structure of the composite.

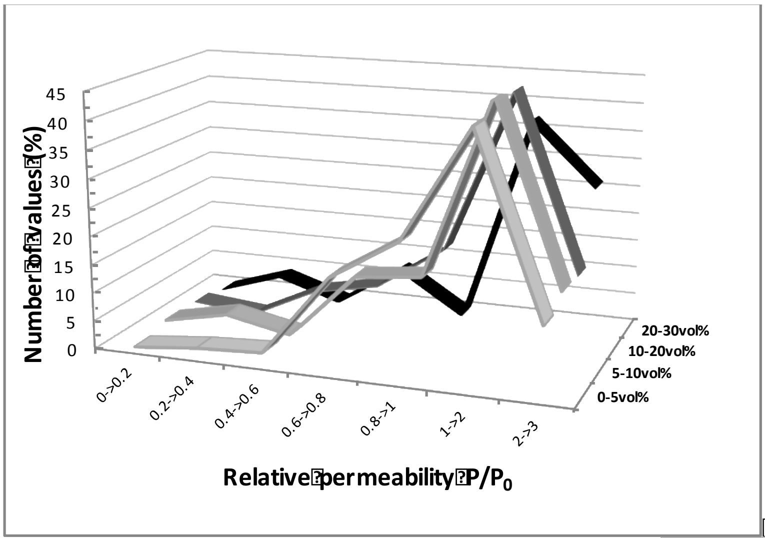

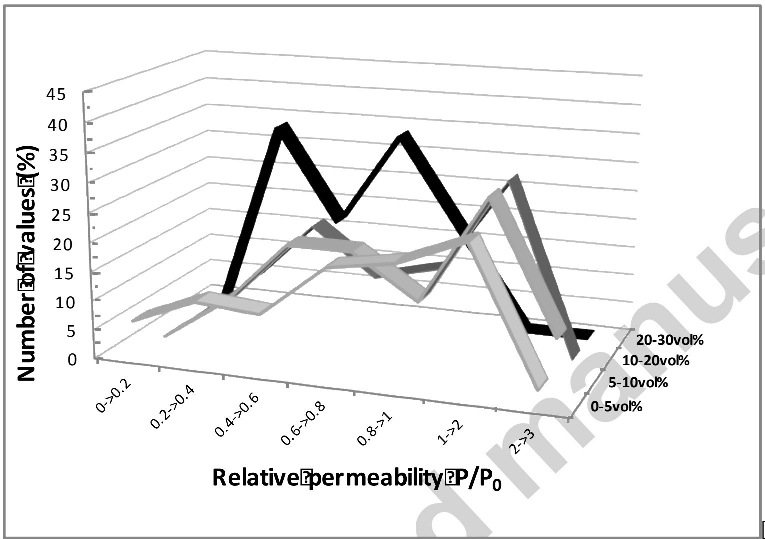

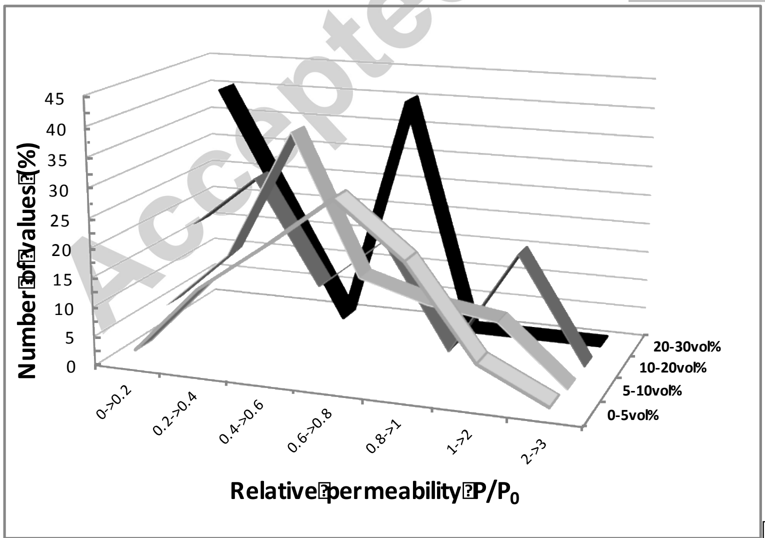

Figure 5: Percentage of permeability values collected for nanocomposites filled with spheres (a), cylinders (b) and platelets (c) -based composites according to the volume filler content and as a function of the relative permeability P/P_0

4. In-depth investigation and understanding of the mass transfer properties/structure relationships in nanocomposites

In the following section, a case by case qualitative explanation of the modulation of the permeability according to particle morphology will be proposed by focusing on the nanostructure obtained and its relationship with mass transfer properties. Three cases will be considered: (1) "ideal" case of monotonic decrease of P/P_0, (2) monotonic increase of P/P_0 and (3) non-monotonic variation of P/P_0. A critical discussion relying on the mechanisms proposed by the different authors will be offered.

4.1. Monotonic decrease of the permeability

Theoretically, the incorporation of impermeable particles displaying a good compatibility with the polymer matrix should favor the decrease of the permeability of gases and water vapor through an increase of the tortuous path for the diffusing molecules. Such "ideal" cases were largely observed in data collected from literature, as illustrated on **Figure 3** for a large range of nanoparticles displaying various shapes, either isodimensional, elongated or nanoplatelets. For the sake of clarity, the exhaustive list of these references is in footnote[1]. The amplitude of this

[1] Among studies that observed a decrease of P/P_0, we can cite the following papers:

For spherical particles: TiO_2 [Hu et al. [84]], SiO_2 nanoparticles [Zoppi et al. [50]], Patel et al. [89,90], Vladimorov et al. [44], Vassiliou et al. [45], Zhu et al. [40], Sadeghi et al. [43], Sadeghi et al. [81]]

For elongated nanoparticles: cellulose nanocrystals [George et al. [99]]], cellulose nanowhiskers [Saxena et al. [65], Sanchez-Garcia et al. [105,107], Bilbao-Sainz et al. [51]], cellulose micro-fibres [Fendler et al [174]],

For nanoplatelets: montmorillonites [Gatos et al. [30], Strawhecker et al. [160], Chang et al. [63,144], Xu et al. [169], Choi et al. [118], Chien et al. [116,175], Yeh et al. [170], Herrera-Alonso et al. [128,176], Katiyar et al. [134], Alboofetileh et al. [110], Abdollahi et al. [109]], rectorite silicate [Wang et al. [177]], mica silicate [Sanchez-Garcia et al. [178],

decrease largely depends on the particle shape and/or particle volume fraction used. The authors mainly attributed this result to (1) a tortuosity effect induced by the nanostructure created by the incorporation of an impermeable particle, and to a lesser extent to (2) the modification of the polymer matrix properties by the presence of nanoparticles, or (3) the modification of the availability of specific sorption sites for the sorption of the diffusing molecule. These three assumptions will be discussed in the following paragraphs.

4.1.1. Tortuosity effect.

When impermeable nanoparticles are incorporated within a polymer matrix, they act as an obstacle to the diffusion and thus the permeation of diffusing molecules, which have to follow a more tortuous pathway. Mathematically, tortuosity (τ) represents the ratio of the distance that a molecular specie must follow through the nanocomposite thickness to the distance through the neat polymer.

This tortuosity effect is influenced by the volume fraction and the dispersion and distribution states of nanoparticles within the polymer matrix. Concretely, it could be related to two quantitative parameters, i.e. the in-situ size aspect ratio of the particle and the orientation of nanoparticles.

cellulose nanocrystals [Fortunati et al. [125]], waxy maize starch nanocrystals [Angellier et al. [113]], boron nitride [Swain et al. [161], Kisku et al. [136]] or silicon carbide [Kisku et al. [137], Dash et al. [120]].

***In-situ* particle aspect ratio.**

The size aspect ratio of a nanoparticle is defined as the ratio of its longest dimension to its lowest dimension. Considering the different possible shapes of nanoparticles, it is obvious that the size aspect ratio of a sphere, equal to 1, is lower than that of elongated nanoparticles and nanoplatelets for which very high size aspect ratio could be achieved.

The achievement of high size aspect ratios theoretically favors the establishment of a more tortuous pathway. This effect is all the greater for nanoplatelets that allow the creation of 2D obstacles. This has been experimentally validated by Gatos et al. [30] who prepared by melt processing fully-exfoliated nanocomposites from a hydrogenated acrylonitrile butadiene rubber polymer and two layered silicates displaying different sizes, *i.e.* octadecylamine modified montmorillonites with a size aspect ratio of 100 and synthetic fluorohectorite with a size aspect ratio of 200. They observed that the highest decrease of oxygen permeability was achieved using the fluorohectorite as filler, which was ascribed to its higher aspect ratio [30]. It must be noted that the achievement of such high *in-situ* size aspect ratios is exceptional. Indeed, the formation of stacks or tactoïds within the polymer matrix is usually obtained due to the agglomeration and/or incomplete exfoliation of nanoplatelets, resulting in a decrease of the theoretical size aspect ratio. An intercalated nanocomposite structure is thus less tortuous than a full-exfoliated structure. This implies that the *in-situ* size aspect ratio is usually different from the one of the native nanoparticle. As an example, Angellier-Coussy et al. [31] found average values of *in-situ* size aspect ratio of 17 and 23 for 10.8 and 2.2 vol% of filler, respectively in wheat gluten/montmorillonite based nanocomposites while the size aspect ratio of one native nanoparticle was about 80. This issue is the same for elongated nanoparticles where agglomeration often occurs.

In practice, the knowledge of the *in-situ* size aspect ratio is thus necessary to fully understand and predict the impact of tortuosity on mass transfer properties. It is usually evaluated using image

analysis of TEM pictures when nanoparticles can be easily distinguished from the matrix as is the case for montmorillonite [31]. This analysis is tricky and time consuming. Indeed, a large number of images must be analyzed to obtain a significant representativeness of the whole material. In addition, it is well-known that TEM analysis has some inherent limitations due to the fact that it projects three-dimensional (3D) objects onto a two-dimensional (2D) plane, resulting in TEM cross-sections that do not necessarily represent the actual size of all the platelets [32]. Furthermore, an ideal image would exhibit sharp transitions from black to white, what is not the case in reality, necessitating the conversion of the original gray-scale TEM micrograph into a black and white image using a semi-automated approach, this step being inevitably accompanied by errors. And finally, this evaluation must be done for each filler content, since the dispersion state strongly depends on the filler content. All these limitations probably explain why the evaluation of the *in-situ* size aspect ratio is rarely experimentally determined. It is usually an imprecise, unrealistic (if the size aspect ratio of the native nanoparticle is considered) or missing data.

***In-situ* size aspect ratio and dispersion state**.

As explained above, the *in-situ* aspect ratio strongly depends on the particle dispersion state. Contrary to the *in-situ* size aspect ratio, which is rarely determined, the impact of the particle dispersion state on nanocomposite mass transfer properties has been largely demonstrated. For example, Koh et al. [33] demonstrated with PLA/organo-modified montmorillonites nanocomposites that the highest decrease of the oxygen and carbon dioxide permeability was obtained for the most exfoliated structure. The same positive impact of exfoliation on permeability decrease was also obtained by Sanchez-Garcia et al. [34] in PHBV-PCL nanocomposites and by Sun et al. [35] for α-zirconium phosphate/epoxy resin nanocomposites.

It is worth noting that the achievement of a good dispersion state is all the more difficult as the filler content increases due to agglomeration phenomena, as evidenced in many systems such as agar- (Rhim et al. [36]), polyester- (Bharadwaj et al. [37]), polyamide- (Picard et al. [38]) or

polyimide- (Chang et al. [39]) based nanocomposites with montmorillonite as nanoparticles. Chemical modification of nanoparticles does not always prevent agglomeration, as evidenced by Zhu et al [40] with modified SiO_2 particles in poly (vinyl chloride) matrix.

Orientation.

To obtain an optimal decreasing effect on permeability, the largest surface of each nanoparticle must be oriented perpendicular to the direction of the gas diffusion or permeation. Well-oriented and aligned particles perpendicularly to the permeation flux have more impact on the decrease of the permeability than disoriented particles as regards the tortuosity effect. This effect of orientation is only valid for elongated particles and nanoplatelets and, of course, all the more significant for particles with high size aspect ratios. This effect of orientation is also theoretically much more efficient for nanoparticles displaying high size aspect ratio in two dimensions (such as platelets) than only in one dimension (such as elongated particles). In practice, it is an extremely challenging task to achieve a regular arrangement of nanoparticles within the polymer matrix. It is strongly dependent on processing methods. Solution intercalation and in-situ-polymerization are more prone to produce nanostructures with well-aligned and oriented particles than melt intercalation as observed by several authors. It is all the more difficult that particles display high aspect ratio in 2-dimension such as platelets. For example, Messersmith et al. [41] showed that montmorillonites adopted a planar orientation in the poly(ε-caprolactone) polymer matrix after in-situ-polymerization and solution casting processing while Sanchez-Garcia et al. [42] noted that it was difficult to obtain, using melt processing and compression molding, well aligned and oriented montmorillonites in PHBV-PCL polymer and that a random orientation is at best the most often achieved.

4.1.2. Modification of the polymer matrix.

The incorporation of nanoparticles can modify the structure and thus the mass transfer properties of the polymer matrix itself. The two main structural modifications reported to contribute to the decrease of P/P_0 are (i) a reduction of polymer free volume associated to an increase in the glass transition temperature and/or (ii) an increase in crystallinity due to a nucleating effect of nanoparticles. The effect of polymer free volume was for example evidenced in the study of Sadeghi et al. [43] by a reduction of the polymer chain mobility in the amorphous phase in the case of polyurethane-silica nanocomposites. The impact of nanoparticles on polymer crystallinity was largely reported for either spherical particles such as silica nanoparticles (Vladimirov et al. [44]; Vassiliou et al. [45]) or layered particles such as montmorillonite (Sanchez-Garcia et al. [42]; Ghasemi et al. [46]). Crystallites act as obstacles to migrant diffusion.

4.1.3. Decrease of polymer sorption sites.

The chemical modification of the nanoparticle surface is generally performed to reach a better filler/matrix affinity and thus a better dispersion of nanofillers within the polymer matrix. A side effect of this higher affinity is a decrease of the availability of the sorption sites in the polymer. It is particularly true for highly interactive molecules such as water vapor that interacts though hydrogen bonding with hydrophilic sites. These sites bonded with the nanoparticles are not any more available for water sorption. Such changes in specific interactions between the migrant and the polymer were proposed to explain the decrease of water vapor permeability observed by Tunc et al. [47] in wheat gluten/montmorillonite or by Lee et al. [48] in soy protein/montmorillonite nanocomposites.

4.2. Monotonic increase of the permeability

Several assumptions are proposed in literature to explain either the absence of significant modification or even an increase of the permeability in nanocomposites: (1) an insufficient tortuosity effect, (2) the occurrence of macroscopic structural defects in the nanocomposite

material induced for instance by particles agglomeration, (3) a significant modification of the structure of the polymer matrix such as a decrease of crystallinity or molecular weight, and (4) an increase of migrant sorption induced by nanoparticles (case of water vapor for example, for water sensitive materials). It is worth noting that some mechanisms assumed to explain an increase of P/P_0 were previously discussed for explaining a decrease of P/P_0 (§ 3.1).

4.2.1 Lack of tortuosity effect.

In some cases, the dispersion state of nanoparticles did not allow to achieve a sufficient tortuosity effect to slow down the diffusion of migrating molecules, especially for small molecules such as gases. Such an explanation is widely proposed to explain why values of permeability did not change or only slightly decreased in the nanocomposite as compared to the neat matrix. This has been, for example, proposed by Tunc et al. [47] to explain the constancy of O_2 permeability in wheat gluten/montmorillonite nanocomposites. In the same article, authors however demonstrated that the achieved tortuosity was nevertheless sufficient for decreasing permeability of bigger molecules such as aroma compounds. This highlighted that the nature, molecular weight and/or steric hindrance of the migrant are also key parameters governing the mass transfer properties in nanocomposites.

4.2.2. Macroscopic structural defects

Particle agglomeration.

The presence of both nano- or micro-sized agglomerates and aggregates of particles could induce macroscopic structural defects, which play a major role in the increase of P/P_0, as already shown for either spherical-based composites with SiO_2 [Cornelius et al. [49]], TiO_2 nanoparticles [Zoppi et al. [50]] or cylinder-based composites with cellulose fibrils [Bilbao-Sainz et al. [51]]. These agglomeration phenomena are related to a bad dispersion of the nanoparticles which is mainly ascribed to (1) mismatching of the particle polarity, as compared to that of the polymer, resulting

in a low affinity between constituents and thus a poor particle/polymer adhesion [50] and/or (2) inefficiency of the elaboration technique to separate aggregates.

For example, insufficient shearing forces during the melt processing could cause agglomeration of particles. During casting, sol-gel method and in-situ polymerization, coalescence of the particles during drying of the solution could appear through insufficient particle/particle interactions ("bad compatibility"). This last phenomenon is normally limited by chemical modification of the surface of the particles. But when the effect of this chemical modification is wrongly anticipated it could even amplify/trigger coalescence of particles as evidenced by Zhu et al. [40] in their study of H_20 and O_2 permeability of silica/PVC nanocomposites with SiO_2 surface grafted with polymethyl methacrylate (PMMA). They noticed that high content of filling (> 2.5 vol/vol%) increased the permeability of both O_2 and H_20 due to an agglomeration phenomenon owing to the tendency of nanoscale silica modified nanoparticles to be fused together at this concentration. This phenomenon was not anticipated.

Agglomeration could lead to the formation of "interfacial voids" at the particle/polymer matrix interface and to the formation of a preferential pathway for the migration of the molecular penetrant [Ismail et al. [52], Rafiq et al. [53]]. This is further detailed below in the section dedicated to the "interphase".

Interphase.

An interphase, i.e. a "third compartment" with its own properties, is generated at the particles/polymer interface due to the establishment of either weak or strong interfacial interactions between the particles and the polymer matrix. Depending on its nature and thickness (or volume fraction), the interphase could significantly participate to the overall mass transfer properties and strongly influence the overall permeability of the composite as evidenced by Liang et al. [54] in their poly(ethersulfone)/montmorillonite nanocomposites. These authors

hypothesized that the interphase in their nanocomposite structure was made of interface voids due to a poor adhesion between hydrophilic nanoparticles and hydrophobic polymers contributing to the high gas permeability observed.

4.2.3. Modification of the polymer matrix.

The incorporation of nanoparticles could result in the disruption of polymer chain packing, causing an increase of polymer matrix free volume. This increase in free volume leads to an increase in permeability or to a lesser decrease than expected. This impact on free volume is often just a hypothesis that is not always confirmed experimentally, due to the difficulty to experimentally access such information.

Such hypothesis of polymer matrix modification with increase of free volume was speculated by several authors for isodimensional particles-based composites with titanium dioxide [Matteucci et al. [55], Moghadam et al. [56]] or silica nanoparticles [Dougnac et al. [57], Romero et al. [58]] and in elongated particles-based nanocomposites with carbon nanotube [Murali et al. [59]]. An increase of free volume was also hypothesized to occur when using compatibilizing agents due to bad compatibility between the compatibilizer and the surface treated particles (Mittal et al. [60]). The addition of nanoparticles in a polymer matrix could also hinder the crystallization process if chain mobility is hindered, leading thus to a decrease of the overall crystallinity of the polymer that could contribute to enhance the overall mass transfer within the composite [Dougnac et al. [57]].

We noted that this increase of free volume is often considered as a global explanation resulting from different phenomena: in addition to the modification of polymer matrix, increase in free volume could also result in void space formation by nanoparticles aggregation and weak interaction between polymer–nanoparticles at interface [Moghadam et al. [56]]. All these mechanisms are not easily distinguished. Therefore, authors stressed an overall increase of free

volume that they experimentally assessed by density measurements, without distinguishing all underlying mechanisms. Indeed, if the density of the nanoparticles, crystalline polymer and amorphous polymer phases has their pure component values in the nanocomposites, then the density of a nanocomposite sample, would be equal to the theoretical additive density. The difference between theoretical and experimental densities can be rationalized by the overall increase of free volume as evidenced by [Matteucci et al. [55]] in spherical-based composites with titanium dioxide.

4.2.4. Increasing migrant sorption.

The increase of P/P_0 could be related to the establishment of specific interactions between the molecular penetrant and the material constituents, as largely observed for water vapor and hygroscopic nanoparticles such as silica nanoparticles [Bracho et al. [61], Dougnac et al. [57]] or microcrystalline cellulose [Dogan et al. [62]], and also for O_2 and organo-modified montmorillonite [Chang et al. [63]], for O_2 or modified silica nanoparticles [Iwata et al. [64]] or CO_2 and titanium dioxide nanoparticles [Matteucci et al. [55]].

Different mechanisms could occur concomitantly, explaining why significant effects on P/P_0 are not systematically observed. For instance, Dogan et al. [62] did not notice any significant change of the water vapor permeability in hydroxyl propyl methyl cellulose/microcrystalline cellulose nanocomposites in spite of a tortuosity effect. This was ascribed to the occurrence of a competitive effect, *i.e.* an increased water affinity with the materials. The same happened in the study of Matteucci et al. [55]: they observed an enhancement of CO_2 permeability in spherical-based composites with titanium dioxide due to an increase in gas solubility in the nanocomposite films upon incorporation of highly sorbing nanoparticles into the polymer. This effect is overlapping with the creation of voids and global increase in free volume with increasing particle loading. It should be noted that all these explanations are always hypotheses that are usually not experimentally validated.

Figure 6 is providing summary of the two previous 4.1 and 4.2 paragraphs with key take home messages about the main mechanisms explaining monotonic increase of decrease of the ratio P/P_0.

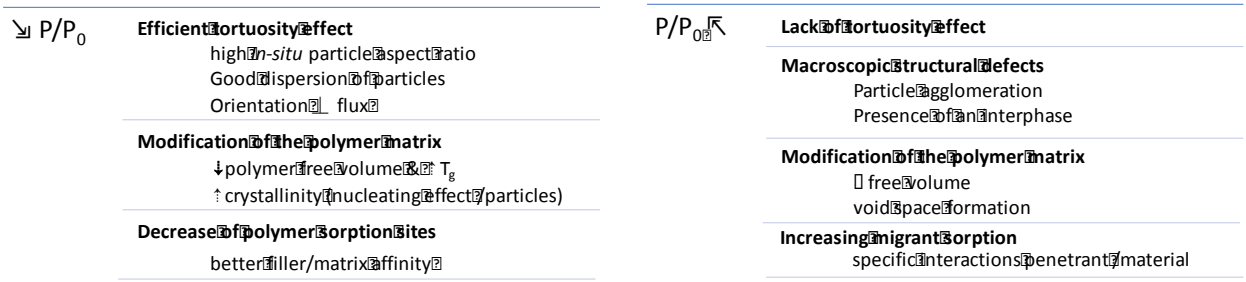

Figure 6: Main mechanisms explaining monotonic increase of decrease of the ratio P/P_0 in nanocomposites

4.3. Non-monotonic variation of P/P_0

The permeability towards gases and water vapor did not always monotonically vary. In a general manner, theories already provided above for explaining monotonic decrease or increase of P/P_0 remain valid in that case and apply to a specific part of the curve.

The most observed non-monotonic variation of P/P_0 is first a decrease of P/P_0 until reaching a threshold value of filler content, followed by a sudden increase of P/P_0. This evolution is generally ascribed to a change in the nanostructure as a function of filler content. For example, in the work of Sanchez-Garcia et al. [42] dealing with montmorillonite-based nanocomposites, the permeability first decreased due to a tortuosity effect and then increased for filler contents higher than 5 vol% due to the formation of agglomerates. In the case of elongated particles-based nanocomposites [Dogan et al. [62], Saxena et al. [65], Paralikar et al. [66]], a similar evolution was observed with the formation of particle agglomerates at higher particle volume fractions (generally > 10 vol%). In addition to agglomeration that could reverse the trend of variation of P/P_0, some extensive cracking of the composite film could occur and lead to a complete loss of

barrier properties [Chaiko et al. [67]], which was attributed by the authors to excessive particle agglomeration at high particle fraction.

An opposite evolution has been also noted in the case of water vapor as migrant: first, an increase of the water vapor permeability probably caused by enhanced affinity between water vapor and composite constituents displaying a hydrophilic nature and, second, a decrease of the permeability induced by the tortuosity that finally is sufficient enough at high loading rates to decrease the permeability value. This has been observed by Follain et al. [68] for poly(ε-caprolactone)/cellulose nanocrystals.

4.4. Explanation of the evolution of the permeability in line with the evolution of solubility and diffusivity coefficients

In this section, it is considered that the properties of the polymer matrix are not affected by the incorporation of nanoparticles and that nanocomposites are two-phases systems with a perfect adhesion at the particle/matrix interface. This makes the relation P=D×S, where P, D and S are respectively the permeability, diffusion and solubility coefficients, valid [49,69]. In order to explain the complex evolution of P/P_0 as a function of filler content, some authors tried to decompose the permeability into diffusivity and solubility and to relate the apparent evolution of P/P_0 to change in D or S or both. For that purpose, they generally determined the diffusivity and/or solubility coefficients independently of the permeability.

In nanocomposites, a decrease in permeability should be ideally related to a decrease in both diffusivity and solubility coefficients due to the formation of a more tortuous pathway (influence on D) and to the diminution of the volume for the sorption of gases or vapors. However, this ideal case was not always observed. In most cases, solubility did not systematically decrease and tended either to remain constant or even to increase.

For example, O_2/CO_2 solubility was found to remain constant in poly(amide-6-b-ethylene oxide) [70] or brominated poly(2,6-diphenyl-1,4-phenylene oxide) [71] filled with silica nanoparticles while CO_2 solubility was found to increase with the addition of silica particles in polybenzimidazole [72]. Despite the fact that the same nanoparticle was used in these three studies, the effect on gas solubility obtained was not. This demonstrated that if the particles could be considered as impermeable (D=0), it is not true for their solubility. As mentioned above in § 3.2, increase of S could also be related to the progressive uncovering of active sorption sites in the polymer matrix as a consequence of particle addition and to the creation of specific sites at the particle/polymer interface that favor the sorption of molecular penetrants as hypothesized by Sadeghi et al. [72] and Suzuki et al. [73].

As regards the diffusivity coefficient, the expected behavior is a decrease due to the restriction of the motion of molecular penetrant and the creation of a more tortuous path caused by the presence of the particles [72,73]. But the opposite phenomenon could also occur. Sadeghi et al. [74], seeking to understand the increase of the permeability in polyvinyl acetate with the addition of silica nanoparticles, made the assumption that the diffusivity coefficient could increase either due to a reduction of the packing density of the polymer which provides further open structures for the diffusion of CO_2 or to a reduction of the crystallinity which lead to more amorphous phases where diffusion happens. The latter effect was also hypothesized by Kono et al. [75] and Ahn et al. [76] on silica nanoparticle based nanocomposite. The diffusivity could also remain constant or increase with the addition of impermeable particles due to bad adhesion or compatibility between constituents or the creation of interconnected cavities/channels as evidenced by Suzuki et al. [73], Kim et al [70] (2001) and Cong et al. [71].

To sum up, following analysis of all aforementioned experimental evidences, we can conclude that there is generally a competition between an increase of the solubility and a decrease of the diffusivity. Therefore, non-monotonic changes of P/P_0, in peculiar, decrease of P/P_0 followed by

an increase for higher particle volume fraction, could be generally ascribed to an increase of S that could, from a threshold value of particle volume fraction, counteract the decrease of D.

4.5. Discussion of the selective transport characteristics of nanocomposite membranes

In the context of developing barrier films, it is also interesting to discuss the selective transport characteristics of nanocomposites membranes. It is indeed of high interest in many applications to develop nanocomposites that are designed to provide a very strong barrier to one component (for instance oxygen) while remaining permeable to another (such as carbon dioxide or water vapor). In this purpose, CO_2/O_2 selectivity and H_2O/O_2 selectivity were calculated, when possible, from the data gathered in the framework of this study and plotted as a function of the nanoparticle volume fraction (**Figures 7** and **8**). In most of cases, CO_2/O_2 and H_2O/O_2 selectivity was not initially in the objective of the original works used to derive it. Therefore, it was not systematically possible to calculate it from the permeability data available per reference. It must be noted that for the sake of clarity, for H_2O/O_2 selectivity, the ratio of nanocomposite selectivity to neat polymer selectivity is used in **Figure 8** while absolute values of PCO_2/PO_2 are directly plotted in **Figure 7**, because they display less range of variation.

As it can be seen in **Figure 7**, and in the logic of result of the Figure 3 analysis, there are much more data of CO_2/O_2 permselectivity available for layered particles than for iso-dimensional particles and elongated ones where only four references have permitted to calculate this value. It is thus not possible to draw meaningful conclusions about the evolution of CO_2/O_2 permselectivity for elongated nanoparticles-based nanocomposites (**Figure 7b**).

Logically, CO_2/O_2 permselectivity of layered particles-based nanocomposites was centered around a mean value of 4, which is usually the permselectivity of oil-based polymers used as neat matrix in most of the studies (**Figure 7c**). In most cases, this permselectivity did not change so much as a function of the nanoparticle volume fraction (up to 8 vol/vol% for the study of Jacquelot et al

[77]) suggesting that the addition of layered nanoparticles would not affect the CO_2/O_2 permselectivity of the nanocomposites and that this property would remain governed by the matrix properties even in nanocomposites. Two studies nevertheless lead to an increase of the CO_2/O_2 permselectivity as a function of nanoparticle volume fraction [78,79]. In the work of Meera et al [79], the decrease of permeability as a function of filler content is much higher for O_2 than for CO_2 leading to an increase of CO_2/O_2 permeability ratio while it seems to be the contrary for Merinska et al [78]. In the same time and for another combination of filler / polymer (Nanofill 5 as MMT/PP), the data of Merinska et al [78] permitted to obtain a decrease of CO_2/O_2 permselectivity. Alena et al [80] also observed either an increase or decrease of CO_2/O_2 permselectivity depending on the type of nanoparticle (MMT) used in LDPE matrix. These last features confirm the random nature of the evolution of CO_2/O_2 permselectivity as a function of nanoparticle volume fraction. We noted that this notion of permselectivity and its evolution as a function of filler content was never explained nor even highlighted by the aforementioned group of authors.

For isodimensional particles-based nanocomposites, the CO_2/O_2 permselectivity is also centered around a value of 5 (**Figure 7a**) and kept almost constant as a function of filler volume fraction. Nevertheless, a group of 5 studies displays very high CO_2/O_2 permselectivity (> 15). Among this group of studies, we noted a general trend toward an increase of permselectivity with nanoparticle volume fraction (4 studies [43,70,81,82] observing an increase against only one [50] observing a decrease). Variation of CO_2/O_2 permselectivity in the aforementioned studies was principally due to the fact that O_2 and CO_2 permeability did not decrease as much as a function of filler content resulting in a non-constant PCO_2/PO_2 ratio. Results of Zoppi et al [50] and Kim et al [70] with high CO_2/O_2 permselectivity were obtained on PEBAX® (copolymer with polyamide-6 and poly(ethyleneoxide)) which is known to display high CO_2/O_2 selectivity in packaging application. These authors did not try to explain why the CO_2/O_2 permselectivity varied in their sample: Kim et al [70] focused only on CO_2/He, CO_2/N_2 and O_2/N_2 selectivity and did not notice

any variation of these selectivities as a function of nanoparticle volume fraction (about 6 for CO_2/He, 70 for CO_2/N_2 and 3 for O_2/N_2 respectively) ; Zoppi et al [50] focusing on O_2/N_2, CO_2/CH_4, CO_2/N_2 and CO_2/H_2 selectivity did not notice so much variation of this value as a function of nanoparticle content except for very high volume ratio (15 vol/vol%). Only Semsarzadeh et al [82] calculated the CO_2/O_2 permselectivity in their study on polyurethane–silica/polyvinyl alcohol mixed matrix membranes. They noticed that by increasing the silica content in membranes, all gas permselectivities including CO_2, namely CO_2/N_2, CO_2/CH_4 and CO_2/O_2 increased much more than selectivity including other gases such as O_2/N_2, up to 136, 69 and 47 %, respectively. They explained that, while O_2, N_2 and CH_4 displayed decreasing permeability, CO_2 permeability demonstrated an increase upon increasing silica content due to an increase in the number of the active sites (polar OH groups) for gas dissolution in polymer matrix. The same reduced decrease in CO_2 permeability compared to other gases such as O_2 or N_2 was observed by Sadeghi et al [43,81] in polyether-based polyurethane–silica and polyurethane-silica nanocomposite leading to moderate increase of CO_2/O_2 selectivity as a function of nanoparticle content (**Figure 7a**).

The comparative examination of permeability and selectivity variation of data collected in the database considered in this work is now in order. Indeed, for the case of inclusion of impermeable particles in a permeable polymer matrix, the anticipated mechanism of induced tortuosity in path of gas molecules is expected to reduce the permeability of different gases by the same extent. A further analysis was thus performed to explore possible correlation between relative permeability and permselectivity in the available set of data. The examination is confined to the case of CO_2/O_2 selectivity in nanocomposite obtained from the inclusion of isodimensional or platelet shaped nanoparticles, as only for those cases is a sufficient number of data available to insure the significance of the statistical analysis. In **Figure 9** the relative permeability for CO_2 in the nanocomposites is related to the corresponding square variation of permselectivity δ defined as follows:

$$\delta = \left(\frac{\alpha_M}{\alpha_{NC}} - 1 \right)^2 \quad \textbf{[2]}$$

where α_{NC} and α_M are CO_2/O_2 permselectivity in nanocomposite and neat matrix, respectively. Despite the scattering, data in **Figure 9** put in evidence that, both for the case of isodimensional particles and platelets, relative permeability higher than one is typically accompanied by a significant deviation of nanocomposite permselectivity from the value of neat matrix, while an interval exists for relative permeability of nanocomposite moderately lower than 1, for which the deviation in permselectivity from the value of neat matrix is negligible. Significantly, the above interval for relative permeability extends to lower values for the case of nanocomposites including platelets with respect to the case of isodimensional particles. It can be thus concluded that a good number of studies considered in this work shows results which are at least qualitatively consistent with the picture resulting from the tortuosity effect induced by the dispersed phase to the motion of gas molecules. On the other hand, a large number of nanocomposites exhibiting either relative permeability values higher than one or very low seems to be often characterized by significant variation of the permesectivity, indicating the relevance of additional phenomena hiding the effect of a pure increase in tortuosity path for the motion of gas molecules in the system.

As it can be seen in **Figure 8**, data available to calculate H_2O/O_2 selectivity are much scarcer than for CO_2/O_2 and, for this reason, the correlation between relative permeability and deviation of permselectivity is not discussed here for this kind of data. No values were even found in the collected references for calculated H_2O/O_2 selectivity in iso-dimensional nanoparticle based nanocomposites. Only three references were found for elongated ones. O_2 permeability is rarely investigated concomitantly to H_2O permeability although H_2O/O_2 selectivity is a very important value in many applications such as packaging where sometimes a high barrier property to O_2 is

required at the same time as low barrier to H_20. From **Figure 8**, it can be concluded that the H_2O/O_2 selectivity did not vary so much as a function of nanoparticle volume fraction except for the study of Kasirga et al [74], Chang et al [39] and Lee et al [48] where H_2O/O_2 selectivity tended to dramatically increase then decrease for at least Chang et al [39] and Lee et al [48]. Even if none of these authors intentionally measured nor explained the evolution of H_2O/O_2 selectivity, this behavior could be generally ascribed to a better tortuosity effect obtained for H_2O than for O_2 and, for non-monotonic behavior, to nonlinear decrease in permeability with clay loading.

To conclude about the selective transport characteristics of nanocomposites membranes, the previous analysis has highlighted that a correlation exists between permeability and the corresponding selectivity value which could be used to emphasize that deviations from expected behavior for selectivity (either positive or negative variation of selectivity) are often associated with deviations from expected behavior for permeability (very high reduction or increase).

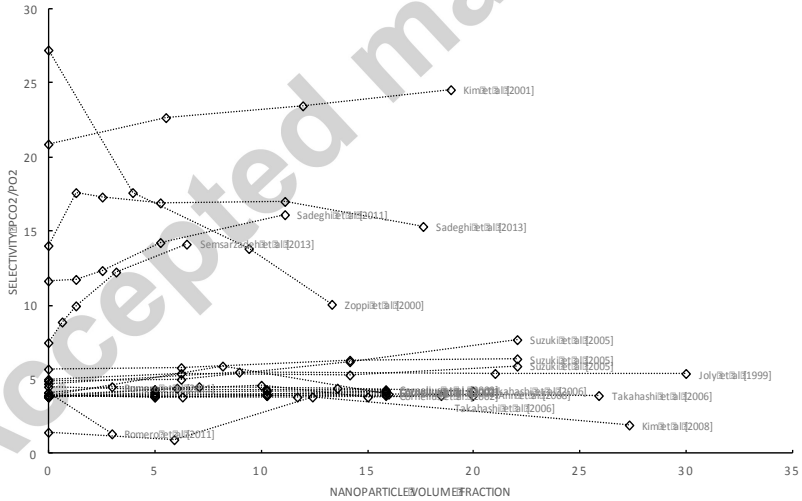

a- Isodimensional particles

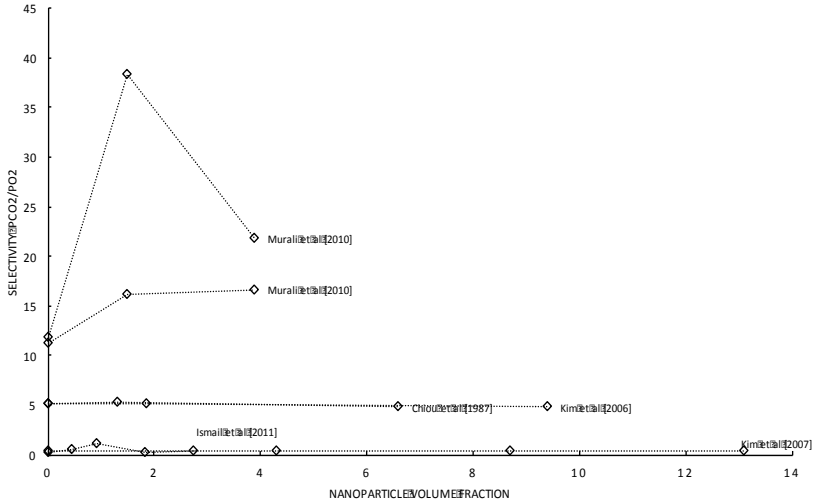

b- Elongated particles

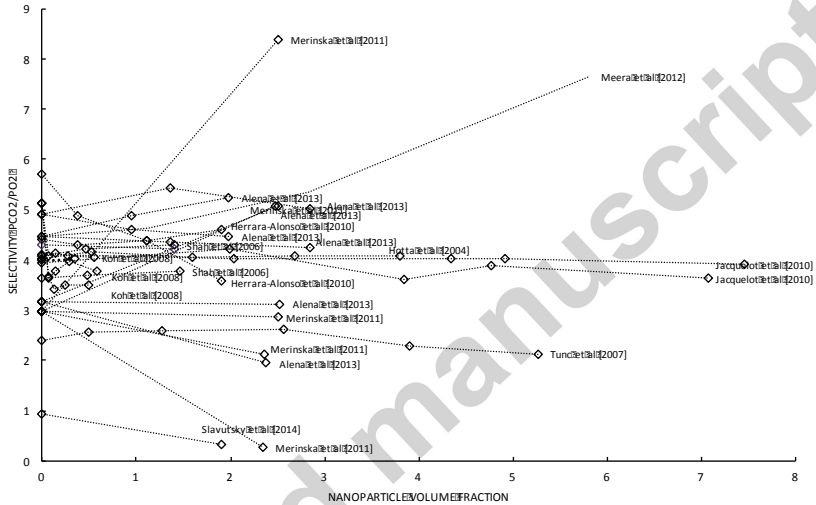

c- Layered particles

Figure 7: Evolution of the CO_2/O_2 permselectivity as a function of particle volume fraction in nanocomposite materials containing either (a) iso-dimensional, either (b) elongate or (c) layered particle

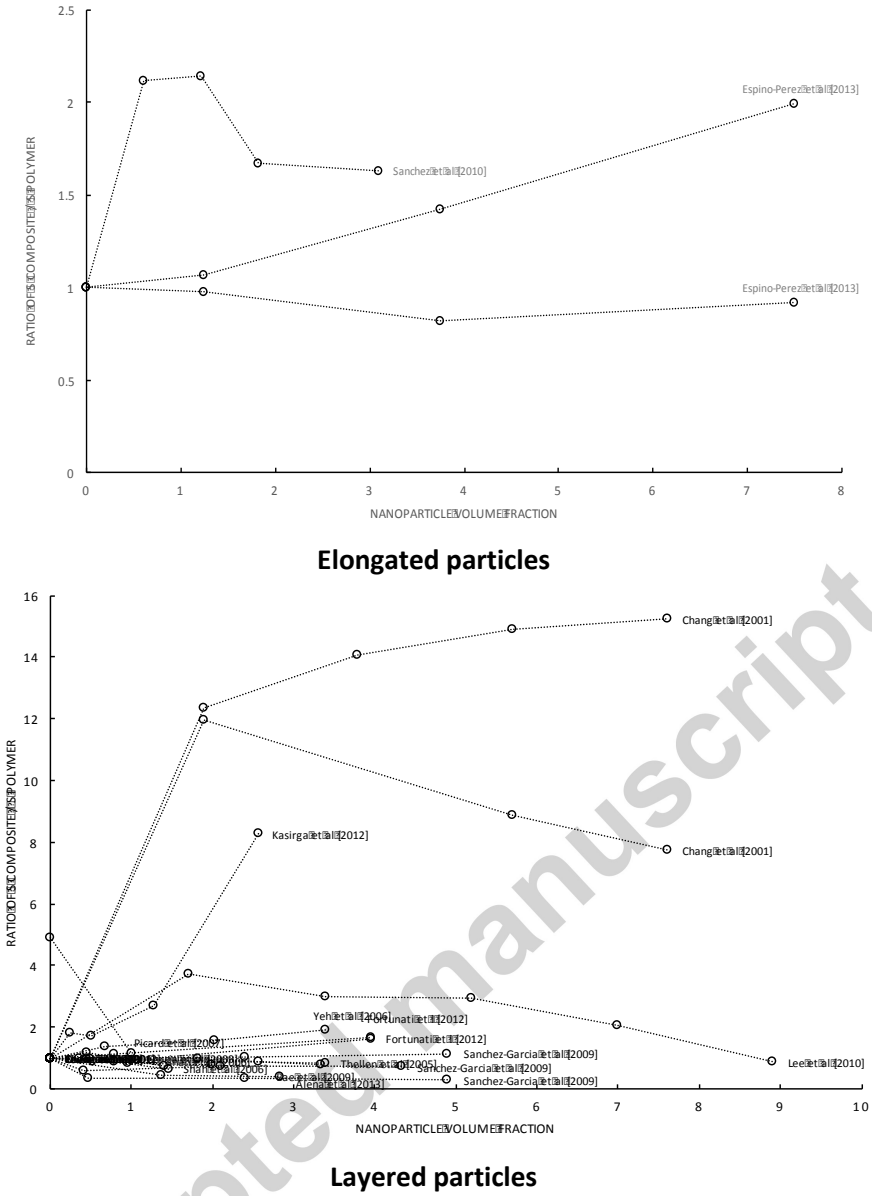

Figure 8: Evolution of the H_20/O_2 selectivity ratio* as a function of particle volume fraction in nanocomposite materials containing either elongated or layered particles

*note that for the sake of clarity, the ratio between selectivity of the nanocomposite to that of the neat polymer was preferred in the representation, instead of true selectivity values

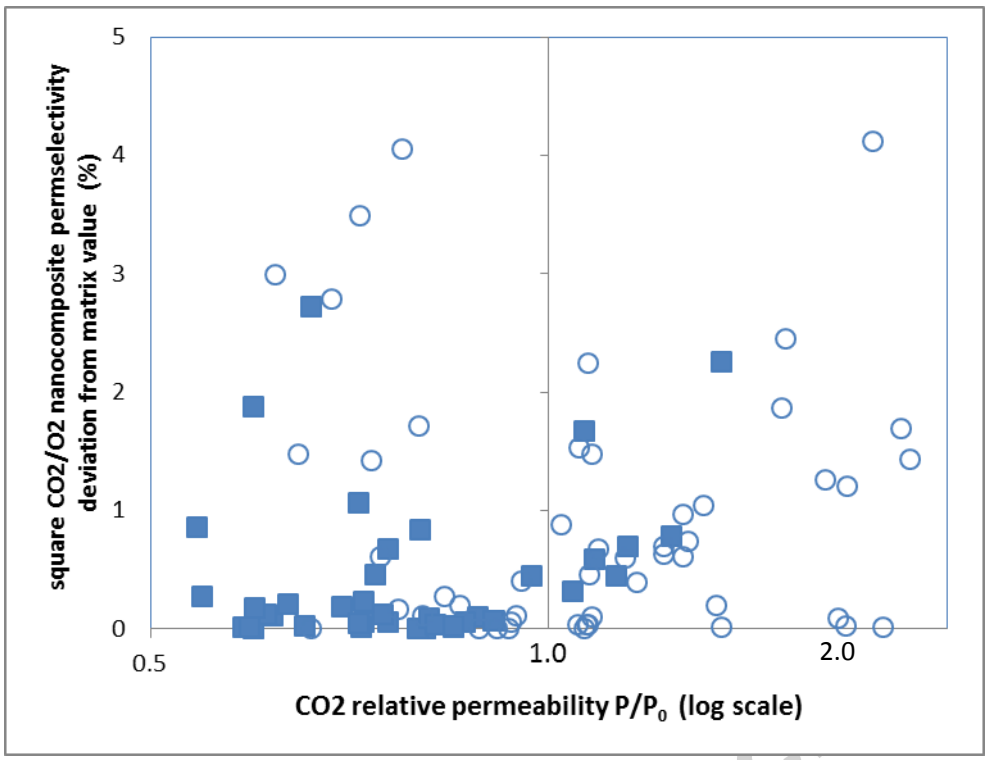

Figure 9: Correlation plot for relative permeability P/P_0 for CO_2 and square deviation of CO_2/O_2 permselectivity in isodimensional particles (open circles) and layered particles (filled squares) nanocomposites.

5. Conclusion

The recently-measured values of gas (O_2, CO_2) and water vapor permeability in agro-, bio- and synthetic-based nanocomposites have been comprehensively reviewed with emphases on the link between their micro- and nano-structure and their barrier performance.

This review has revealed that despite numerous and intensive studies on the optimization of nanocomposite processing and structure in the perspective of modulating their barrier properties, the expected decreasing effect on the permeability is often not so high as expected and somethimes completely the opposite. This review confirmed that layered nanoparticles are more efficient than isodimensional and elongated nanoparticles to decrease the relative permeability

(P/P_0). But, this effect is difficult to anticipate due to numerous interferring mechanisms that provoke modifications of tortuosity, sorption, polymer matrix (crystallinity, free volume, molar mass), creation of an interphase, voids and cracks, and more that lead to unexpected behaviours of the permeability in nanocomposites. Investigation of the selective transport of CO_2 to O_2 and H_20 to O_2 did not reveal a general trend either and it is also difficult to anticipate.

It was concluded that tortuosity, the main mechanism proposed to explain permeability decrease in nanocomposites, often fails in explaining the effect of nanoparticles on nanocomposite barrier properties. This is particlarly important knowing that most of the mathematical models used to predict permeability in nanocomposites are based on this tortuosity effect.

Table 1: Characteristics of the iso-dimensional particles-based nanocomposites of the publications quoted in this review: Nature, size and chemical modification of the particles, processing routes and applications of nanocomposites.

Reference	Particle	Matrix	Size before/after process	Chemical modification	Process	Film thickness	Molecular penetrant	Application
Ahn et al. [76,83]	Silica nanoparticles	Polysulfone (PSF)	11.1-13.3 /	Trimethylsilyl Tetraethoxysilane	Solution / Casting	60 - 80 µm	Oxygen/ Carbon dioxide	Membrane
Bracho et al. [61]	Silica nanoparticles	Poly(propylene)	20 and 100nm /	Trimethylchlorosilane Dimethyloctylchlorosilane	Melt mixing / Thermopressing	1000 µm	Water vapor	General engineering
Cong et al. [71]	Silica nanoparticles	Brominated Poly(2,6-diphenyl-1,4-phenylene oxide)	10nm /	Unmodified Trimethylsilyl Triphenylsilyl	Sol-gel / Solution casting	50 - 90 µm	Carbon dioxide	Membrane
Cornelius et al. [49]	Silica nanoparticles	Poly(imide)	-	Tetraethoxysilane Phenyltrimethoxylane Methyltrimethoxysilane Tetramethoxysilane	Sol gel / Solution casting	80µm	Oxygen / Carbon dioxide	Membrane
Cornelius et al. [49]	Silica nanoparticles	Poly(imide)	-	Phenyltrimethoxylane Methyltrimethoxysilane	Sol gel / Solution casting	80µm	Oxygen / Carbon dioxide	Membrane
Dougnac et al. [57]	Silica nanoparticles	Poly(propylene)	10-150nm /	Tetraethoxysilane	Sol gel / Melt mixing / Pressing	5000 µm	Oxygen	General engineering
Hu et al. [84]	Titanium dioxide nanoparticles	Poly(amide imide)		Unmodified	Sol-gel / Solution casting	15 -17 µm	Oxygen / Carbon dioxide	Membrane
Iwata et al. [64]	Silica nanoparticles	Poly(acrilonitrile)	/ 56.7nm	Tetraethoxysilane	Sol gel / Solution casting	60 - 110 µm	Oxygen	Membrane

Joly et al. [85]	Silica nanoparticles	Polyimide Poly(4,4-oxydiphenylene pyromellitimide)	/ 50-150nm	Tetramethoxysilane	Solution / Casting	25 - 30 µm	Oxygen / Carbon dioxide	Membrane
Kim et al. [70]	Silica nanoparticles	Poly(amide-6-b-ethylene oxide)	/ 33 and 517nm	Tetraethoxysilane	Sol-gel / Solution casting		Oxygen / Carbondioxide	Membrane
Kim and Marand [86]		Polysulfone						
Kong et al. [87]	Titanium dioxide nanoparticles	Poly(imide)	/ 10nm	Unmodified	Sol-gel / Solution casting	-	Oxygen	Membrane

Table 1 (continue) …

Publication	Particle	Matrix	Size before/ after process	Chemical modification	Process	Film thickness	Molecular penetrant	Application
Kono et al. [75]	Silica nanoparticles	Poly(1-chloro-2-phenylacetylene) Poly[1-phenyl-2-(4-trimethylsilyl)phenylacetylene] Poly[1-(trimethylsilyl)-1-propyne]	13 nm /	Trimethylsilyl	Solution / Casting	80 - 120µm	Oxygen / Carbon dioxide	Membrane
Matteucci et al. [88]	Titanium dioxide nanoparticles	1,2 Poly(butadiene)	< 50nm / 9(+/-)4nm	Unmodified	Solution / Casting	180 - 220 µm	Carbon dioxide	Membrane
Moghadam et al. [56]	Titanium dioxide nanoparticles	Poly(imide)	3 nm /	Unmodified	Solution / Casting	80 - 120µm	Oxygen / Carbon dioxide	Membrane
Patel et al. [89]	Silica nanoparticles	Poly(ethylene glycol)	12nm /	Methacrylate	Solution / Casting	40 - 200 µm	Oxygen / Carbon dioxide	Membrane
Patel et al. [90]	Silica nanoparticles	Crosslinked Poly(ethylene glycol)	12nm /	Methacrylate	Solution / Casting	40 - 200 µm	Carbon dioxide	Membrane
Rafiq et al. [53]	Silica nanoparticles	Poly(sulfone) Poly(imide)	/ <100nm	Tetraethoxysilane 3-amino-propyltrimethoxysilane	Solution / Casting	150 µm	Carbon dioxide	Membrane
Romero et al. [58]	Silica nanoparticles	Poly(etherimide)	-	Tetraethoxysilane 3-amino-propyltrimethoxysilane	Solution / Casting	25 - 70 µm	Oxygen / Carbon dioxide	Membrane
Sadeghi et al. [74]	Silica nanoparticles	Poly(ethylene vinyl acetate)	-	Tetraethoxysilane	Sol-gel / Solution casting		Oxygen / Carbon dioxide	Membrane
Sadeghi et al. [72]	Silica nanoparticles	Poly(benzimidazole)	-	Tetraethoxysilane 3-glycidyloxy-propyltrimethoxysilane	Sol-gel / Solution casting	40 µm	Carbon dioxide	Membrane
Sadeghi et al. [81]	Silica nanoparticles	Poly(ether-based polyurethane)	-	Tetraethoxysilane 3-glycidyloxy-propylterimethoxysilane	Sol-gel / Solution casting	100 µm	Oxygen / Carbon dioxide	Membrane
Sadeghi et al. [43]	Silica nanoparticl	Polycaprolactone-based polyurethane	-	Tetraethoxysilane	Sol-gel / Solution casting	100 µm	Oxygen / Carbon dioxide	Membrane

	es			3-glycidyloxy-propylterimethoxysilane				

Table 1 (continue) …

Publication	Particle	Matrix	Size before/after process	Chemical modification	Process	Film thickness	Molecular penetrant	Application
Semsarzadeh et al. [82]	Silica nanoparticles	Polyurethane	-	Tetraethoxysilane /Polyvinyl alcohol	Sol-gel / Solution casting	120 µm	Oxygen / Carbon dioxide	Membrane
Suzuki et al. [73]	Silica nanoparticles	Poly(imide)	-	Tetramethoxysilane	Sol-gel / Solution casting	-	Oxygen / Carbon dioxide	Membrane
Takahashi et al. [69]	Silica nanoparticles	Poly(etherimide)	18-26nm / 11-13nm / 25-31nm /	Methyl Trimethylsilyl Polydiméthylsiloxane	Solution / Casting and Melt processing / Compression moulding	50 - 70 µm / 200 - 300 µm	Oxygen / Carbon dioxide	Membrane
Takahashi et al. [69]	Silica nanoparticles	Poly(etherimide)	-	3-amino-propyltrimethoxysilane	Solution Casting and Melt processing / Compression moulding	30 - 50 µm / 200 µm	Oxygen / Carbon dioxide	Membrane
Ulutan et al. [91]	Silica nanoparticles	Poly(vinyl chlorure)	-	Unmodified	Melt-mixing / Thermopressing	300 - 500 µm	Water vapor	Membrane
Vassiliou et al. [45]	Silica nanoparticles	Isostatic poly(propylene)	12nm /	Unmodified	Melt mixing / Thermopressing	45 - 55 µm	Oxygen	Membrane
Vladimirov et al. [44]	Silica nanoparticles	Isostatic poly(propylene)	12nm /	Unmodified	Melt mixing / Thermopressing	45 - 55 µm	Oxygen	Membrane
Yu et al. [92]	Silica nanoparticles	Poly(sulfone)	/ 16nm / 12nm	Hydroxyl Trimethylsilyl	Solution / Casting	50 nm	Carbon dioxide	Membrane
Zhou et al. [93]	Titanium dioxide nanoparticles	Whey protein	< 20nm /		Solution / Casting	50 µm	Water vapor	Packaging
Zhu et al. [40]	Silica nanoparticles	Poly(vinyl chlorure)	25nm /	3-(Trimethoxysilyl)-propyl methacrylate	Melt mixing / Compression moulding	450 - 550 µm	Oxygen / Water vapor	General engineering
Zoppi et al. [50]	Silica nanoparticles	Poly(ethylene oxide-b-amide-6)	-	Tetraethoxysilane	Sol-gel / Solution casting	-	Oxygen / Carbon dioxide	Membrane
Zoppi et al. [50]	Titanium dioxide nanoparticles	Poly(ethylene oxide-b-amide-6)	-	Tetraethoxysilane	Sol-gel / Solution casting	-	Oxygen / Carbon dioxide	Membrane

Table 2: Characteristics of the elongated particles-based nanocomposites of the publication quoted in this article; information about the nature, the size and the modification of the particles, and overview of the composites processing and applications

Reference	Particle	Matrix	Size before/after process	Chemical modification	Process	Film thickness	Molecular migrant	Application
Azeredo et al. [94]	Cellulose fibre	Mango puree	Length: 82.6(+/-)4.3 nm Diameter 7.2(+/-)0.3 nm	Unmodified	Solution / Casting		Water vapor	Packaging

Azeredo et al. [95]	Cellulose fibre	Chitosan	Length: 98.1(+/-)4.7 nm Diameter 8.0(+/-)3.4 nm	Unmodified	Solution / Casting	29 µm	Water vapor	Packaging
Bilbao-Sainz et al. [51]	Cellulose fibrils Eucalyptus sulphite wood pulp Oxidized cellulose fibrils Softwood cellulose fibre	Hydroxy propyl methyl cellullose	Diameter: 35(+/-)9 nm Diameter: 67(+/-)34 nm	Unmodified TEMPO sodium bromide	Solution / Casting	1150 µm	Water vapor	Packaging
Chang et al. [96]	Cellulose whisker Microcrystalline cellulose Cellulose particle	Wheat starch	Length: 301(+/-)67 nm Diameter: 28(+/-)9 nm 50-100nm /	Unmodified Unmodified	Solution / Casting		Water vapor	Packaging
Cong et al. [97]	Carbon nanotube	Brominated poly(2,6-diphenyl-1,4-phenylene oxide)	Length: 0.1-1 µm Average diameter: 0.8-1.2 nm Length: 0.5-50 µm Average diameter: 40-60 nm	Unmodified	Solution / Casting	50 - 80 µm	Carbon dioxide	Membrane
Dogan et al. [62]	Microcrystalline cellulose	Hydroxy propyl methyl cellullose	Average size 0.5-3µm	Unmodified	Solution / Casting		Water vapor	Packaging
Espino Perez et al. [98]	Cellulose whisker	Poly(lactic acid)	/ Average length: 243.9 (+/-) 48.5 nm Average diameter: 9.4 (+/-) 2.5 nm	n-octadecyl isocyanate	Solution / Casting	40 - 120 µm	Oxygen / Water vapor	General engineering
Follain et al. [68]	Cellulose nanocrystal	Poly(ε-caprolactone)		Long-chain isocyanate	Solution / Casting	300 - 400 µm	Water vapor	General engineering
George et al. [99]	Bacterial cellulose nanocrystal	Food gelatin	Average length: 290(+/-)130 nm Average diameter: 20(+/-)5 nm	Unmodified	Solution / Casting		Water vapor	Packaging

Table 2 (continued …)

Reference	Particle	Matrix	Size before/after process	Chemical modification	Process	Film thickness	Molecular migrant	Application
Ismail et al. [52]	Carbon nanotube	Poly(ethersulfone)	Average inner and outer diameter: 3.5-15 nm	3-aminopropyl-triethoxysilane (APTES)	Solution / Casting		Oxygen / Carbon dioxide	Membrane
Kim et al. [100]	Carbon nanotube	Poly(imide siloxane)	Average diameter: 1.4 (+/-) 0.2 nm	Acid treatment	Solution / Casting		Oxygen / Carbon dioxide	Membrane

Kim et al. [101]	Carbon nanotube	Poly(sulfone)	Average diameter: 1.2 nm	Wet-oxidation Acid treatment	Solution / Casting		Oxygen / Carbon dioxide	Membrane
Mondal et al. [102]	Carbon nanotube	Poly(urethane)	Diameter: 2-15 nm Length: 1-10 µm	Aniline solution diluted in DMF	Solution / Casting	90 µm	Water vapor	General engineering
Murali et al. [59]	Carbon nanotube	Poly(ether-block-amide)	Length: 5-15 µm Diameter: 10-20 nm	Unmodified	Solution / Casting	15 - 20 µm	Oxygen / Carbon dioxide	Membrane
Pantani et al. [103]	ZnO particle	Poly(lactic acid)	Length: up to around 100 nm Diameter: 15-30 nm	Unmodified	Melt compounding / Compression moulding	150 µm	Water vapor	Packaging
Paralikar et al. [66]	Cellulose nanocrystal	Poly(vinyl alcohol) Crosslinked Poly(acrylic acid)	Length: 50-200 nm Diameter: 5-10 nm	Unmodified Free acid	Solution / Casting	10 µm	Water vapor	Membrane
Pradhan et al. [104]	Carbon nanotube	Poly(acrilonitrile)	Length: 0.1-10 µm Diameter: 10-15 nm	Sulphuric and nitric acid	Free emulsion polymerization / Thermopressing	500 µm	Oxygen	General engineering
Sanchez-Garcia et al. [105]	Carbon nanofibre Carbon nanotube	Polyhydroxybutyrate-co-valerate Poly(caprolactone)	Length: 1-10 µm Diameter: 5-20 nm Length: 50-100 µm Diameter: 70-200 nm	Unmodified Unmodified	Solution / Casting	100 µm	Oxygen	Packaging
Sanchez-Garcia et al. [106]	Cellulose whisker	Poly(Lactic acid)	Length: 60-160 nm Thickness: 10-20 nm	Unmodified	Solution casting		Oxygen / Water vapor	Packaging
Sanchez-Garcia et al. [107]	Cellulose whisker	Hybrid Carrageenan	Length: 25-50nm Diameter: 5 nm	Unmodified	Solution / Casting	50 µm	Water vapor	Packaging
Saxena et al. [65]	Cellulosic whisker	Oat spelt xylan	Length: 150-200 nm Width < 20 nm	Sulphuric acid	Solution / Casting	89 - 93 µm	Water vapor	General engineering
Yu et al. [108]	ZnO-carboxymethylcellulose sodium	Glycerol plasticized-pea starch	Length: 30-40 nm	Unmodified	Solution / Casting		Water vapor	General engineering

Table 3: Characteristics of the platelet particles-based composites of the publication quoted in this article; information about the nature, the size and the modification of the particles, and overview of the composites processing and applications

Reference	Particle	Matrix	Size before/after process	Chemical modification	Process	Film thickness	Molecular penetrant	Application
Abdollahi et al. [109]	Montmorillonite	Alginate	Average length: 300nm	Unmodified	Solution / Casting	–	Water vapor	Packaging

Reference	Particle	Matrix	Size before/after process	Chemical modification	Process	Film thickness	Molecular penetrant	Application
Alboofetileh et al. [110]	Montmorillonite	Sodium algenate	Average diameter: 40nm / -	Unmodified	Solution / Casting	40 - 60 µm	Water vapor	Packaging
Alena et al. [80]	Montmorillonite	Linear low density polyethylene Poly(chlorure vinyl)	-	Unmodified Methyl bis-2-hydroxyethyl tallow ammonium Dimethyl, hydrogenated tallow, 2-ethylhexyl quaterny ammonium Methyl, dehydrogenated tallow ammonium	Extrusion / roll-pressing	100 µm	Oxygen / Carbon dioxide / Water vapor	Packaging
Alexandre et al. [111]	Montmorillonite	Poly(amide 12)	/ Thickness: 2-6nm	Methyl bis-2-hydroxyethyl tallow ammonium	Melt processing / Compression moulding	200 - 250µm	Water vapor	Membrane
Ali et al. [112]	Montmorillonite	Starch / Poly(vinyl alcohol)	-	Unmodified	Solution / Casting	–	Water vapor	Packaging
Angellier et al. [113]	Waxy maize starch nanocrystals	Natural rubber	Thickness: 6-8nm Length:40-60nm Width: 15-30nm/ Aspect ratio 16	Unmodified	Solution / Casting	200 - 1000 µm	Oxygen / Water vapor	General engineering
Bae et al. [114]	Montmorillonite	Fish gelatin	-		Solution / Casting	-	Oxygen / Water vapor	Packaging
Balachandran et al. [115]	Montmorillonite	Nitrile rubber	-	Dimethyl dehydrogenated tallow ammonium	Melt processing / Compression moulding	2000 µm	Oxygen	General engineering
Bharadwaj et al. [37]	Montmorillonite	Polyester resin	-	Methyl bis-2-hydroxyethyl tallow ammonium chloride	Melt processing / Compression moulding	-	Oxygen	General engineering
Chaiko et al. [67]	Montmorillonite	Paraffin wax	10-20nm /	1-hydroxydodecane-1,1-diphosphate ammonium salt	Melt processing	50 µm	Oxygen	General engineering
Chang et al. [39]	Montmorillonite	Poly(imide)	-	Dodecylamine ammonium salt Hexadecylamine ammonium salt Methyl bis-2-hydroxyethyl tallow ammonium	Solution / Casting	10 - 15 µm	Oxygen / Water vapor	General engineering
Chang et al. [63]	Montmorillonite	Poly(lactic acid)	/ Thickness: 1-5nm	Hexadecylamine Dodecyltrimethyl ammonium bromide–montmorillonite	Solution / Casting	10 - 15 µm	Oxygen	Packaging
Chien et al. [116]	Montmorillonite	Poly(vinyl acetate)	/ Aspect ratio 320	-	Soap free emulsion polymerization / Casting	150 µm	Water vapor	General engineering
Chivrac et al. [117]	Montmorillonite	Wheat starch	-	Organo-modification	Melt processing /		Water vapor	Packaging

Reference	Particle	Matrix	Size before/after process	Chemical modification	Process	Film thickness	Molecular penetrant	Application
Choi et al. [118]	Montmorillonite	Poly(urethane)	-	Organofier UE400	Compression moulding / Solution / Spin coating	30 -50 µm	Oxygen	General engineering
Choi et al. [119]	Montmorillonite	Poly(propylene)	-	Dimethyl di(hydrogenated tallowalkyl) quaternary ammonium	Melt-compounding / Injection moulding	600 - 800 µm	Oxygen	Packaging
Dash et al. [120]	Silicon carbide	Starch	50nm /		Solution / Thermopressing	500 µm	Oxygen	Packaging
Duan et al. [121]	Montmorillonite	Poly(lactic acid)	Average thickness: 1.6nm Average length:80nm	Methyl bis-2-hydroxyethyl tallow ammonium chlorid	Melt processing / Compression moulding	600 µm	Water vapor	Packaging
Dunkerley et al. [122]	Montmorillonite	Poly(styrene)	-	Dimethyl di(hydrogenated tallowalkyl) quaternary ammonium	Solution spraying	60 - 270 µm	Oxygen	Packaging
Echeverria et al. [123]	Montmorillonite	Soy protein isolate	-	Unmodified	Solution / Casting	75 -90 µm	Water vapor	Packaging
Fasihi et al. [124]	Montmorillonite	Poly(amide 6)	Average particle size 8µm /Aspect ratio 210	Organo-modification	Melt processing / Compression moulding	150 µm	Oxygen	Packaging
Fortunati et al. [125]	Cellulose nanocrystals	Poly(lactic acid)	Length:100-200nm Width: 5-10nm /	Unmodified Acid phosphate ester of ethoxylated nonyphenol	Solution - Casting	150 - 250 µm	Oxygen / Water vapor	Packaging
Gain et al. [126]	Montmorillonite	Poly(e-caprolactone)	-	Unmodified Methyl bis-2-hydroxyethyl tallow ammonium	Melt blending - In situ polymerization / Compression moulding	100 µm	Carbon dioxide	General engineering
Gatos et al. [30]	Fluorohectorite Montmorillonite	Hydrogenated acrylonitirle butadiene rubber	/ Aspect ratio 200 / Aspect ratio 100	Synthetic fluorohectorite Synthetic fluorohectorite / Octadecylamine Quaternary ammonium salt Quaternary ammonium salt / Octadecylamine	Melt mixing / Thermopressing	1000 µm	Oxygen	General engineering
Ghasemi et al. [46]	Montmorillonite	Poly(ethylene terephthalate)	-	Methyl bis-2-hydroxyethyl tallow ammonium	Melt processing / Casting	25 - 90 µm	Oxygen	Packaging
Guo et al. [127]	Montmorillonite	Fish gelatin	-	Unmodified	Solution / Casting	300 µm	Water vapor	Packaging
Herrera-Alonso et al. [128]	Montmorillonite	Poly(n-butyacrylate)	/Average particle diameter 140nm	[2-(Acryloyloxy)ethyl]-trimethylammonium	Emulsion polymerization / Casting	180 - 240µm	Oxygen / Carbon dioxide	Membrane
Herrera-Alonso et al.	Montmorillonite	Poly(n-butyacrylate)	-	[2-(Acryloyloxy)ethyl]-	In-situ polymerizatio	180 - 240µm	Oxygen / Carbon	Membrane

Reference	Particle	Matrix	Size before/after process	Chemical modification	Process	Film thickness	Molecular penetrant	Application
[128]				trimethylammonium	n / Casting		dioxide	
Horst et al. [129]	Montmorillonite	Poly(propylene)	-	Quaternary ammonium salt	Melt-mixing / Injection moulding	140 - 200 µm	Oxygen	General engineering
Hotta et al. [130]	Montmorillonite	Linear low density polyethylene	-	Dimethylbis(hydrogenated-tallow ammonium	Melt processing / Compression moulding	150 µm	Oxygen / Carbon dioxide	General engineering
Huang el al. [131]	Montmorillonite	Poly(imide)	-	Hexadecyltrimethyl ammonium bromide 4,4' - oxydianiline	Solution / Casting / Thermal imidization	60 µm	Oxygen / Water vapor	Membrane
Ito et al. [132]	Montmorillonite	Poly(amide 6)	-	Hexadecyltrimethyl ammonium bromide / 4,4' - oxydianiline 12-aminolauric acid ammonium salt	Extrusion / Compression moulding	200 µm	Oxygen	General engineering
Jacquelot et al. [77]	Montmorillonite	High and low density polyethylene	-	Dimethyl tallow benzyl ammonium	Melt processing / Compression moulding	150 µm	Oxygen / Carbon dioxide	General engineering
Kasirga et al. [133]	Montmorillonite	Chitosan	Mix nano- / micro- <100nm to 2µm		Solution / Casting		Oxygen / Water vapor	Packaging
Katiyar et al. [134]	Montmorillonite	Poly(L-lactic acid)	-	Dimethyl, hydrogenated tallow, 2-ethylhexyl quaterny ammonium	Extrusion / Rolling compression	400 µm	Oxygen / Water vapor	Packaging
	Laureate hydroxide			Unmodified				
Ke et al. [135]	Montmorillonite	Poly(ethylene terephthalate)	-	Organo-modification	Melt mixing - In situ polymerization / Thermopressing	25 µm	Oxygen	Packaging
Kisku et al. [136]	Boron nitride	Chitosan	-		Solution / Thermopressing	500 µm	Oxygen	Packaging
Kisku et al. [137]	Silicon carbide	Cellulose	70nm /		Solution / Thermopressing	500 µm	Oxygen	Packaging
Kim et al. [138]	Montmorillonite	Epoxy resin	-	Quaternary alkylamine Quaternary ammonium salt Octadecylamine	Solution / Casting	1000 - 3000 µm	Water vapor	General engineering application
Koh et al. [33]	Montmorillonite	Poly(lactic acid)	-	Octadecyl ammonium chloride Dimethyl di(hydrogenated tallowalkyl) quaternary ammonium Methyl bis-2-hydroxyethyl tallow ammonium chlorid	Solution / Casting	25-40 µm	Oxygen / Carbon dioxide	Membrane application
Kristo et al. [139]	Starch crystals	Pullulan	Thickness: 6-8nm	-	Solution / Casting	69-75 µm	Water vapor	General engineerin

Reference	Particle	Matrix	Size before/after process	Chemical modification	Process	Film thickness	Molecular penetrant	Application
								g application
Kumar et al. [140]	Montmorillonite	Soy protein isolate	-	Unmodified	Melt processing / Casting	-	Water vpour	Packaging application
Kumar et al. [140,141]	Montmorillonite	Soy protein isolate	-	Dimethyl di(hydrogenated tallowalkyl) quaternary ammonium Methyl bis-2-hydroxyethyl tallow ammonium	Melt processing / Casting	-	Water vapor	Packaging application
Lan et al. [142]	Montmorillonite	Poly(imide)	-	Polyamic acid	Solution - Casting	25 µm	Carbon dioxide	General engineering application
Lavorgna et al. [143]	Montmorillonite	Chitosan	-	Unmodified	Solution / Casting	115 - 125 µm	Water vapor	Packaging application
Lee et al. [144]	Montmorillonite	High density polyethylene	-	Octadecylamine	Melt processing / Compression moulding	50 µm	Carbon dioxide	General engineering application
Lee et al. [145]	Montmorillonite	Poly(methyl acrylate-co-methyl methacrylate)	-	Unmodified	Soap free emulsion polymerization / Casting	200 µm	Water vapor	General engineering application
Lee et al. [48]	Montmorillonite	Soy protein	-	Unmodified	Solution / Casting	90 µm	Water vapor	Packaging application
Liang et al. [54]	Montmorillonite	Poly(ether sulfone)	/ Aspect ratio 7.4 - 20	Unmodified	Solution / Casting	21 -27 µm	Carbon dioxide	Membrane application
Luecha et al. [146]	Montmorillonite	Zein	-	Methyl dihydroxy ethyl hydrogenated tallow ammonium	Solution / Casting Blown - Extrusion	40 - 80 µm	Water vapor	Packaging application
Masclaux et al. [147]	Montmorillonite	Native potato starch	-		Solution / Casting	50 µm	Oxygen	General engineering application
Meera et al. [79]	Montmorillonite	Natural rubber	-	Octadecyl ammonium chloride	Melt processing / Compression moulding	1000 µm	Oxygen / Carbon dioxide	Membrane application
Merinska et al. [78]	Montmorillonite	Poly(ethylene)	-	Methyl bis-2-hydroxyethyl tallow ammonium Dimethyl, hydrogenated tallow, 2-ethylhexyl quaterny ammonium Methyl, dehydrogenated tallow ammonium Organo-modification	Extrusion / Thermopressing	50 µm	Oxygen / Carbon dioxide / Water vapor	Packaging application
Messersmith et al. [41]	Montmorillonite	Poly(ε-caprolactone)	-	Protonated amino acid	Solution / Casting	200 µm	Water vapor	General engineering application
Mittal et al. [148]	Montmorillonite	Poly(propylene)	-	1-decyl-2-methyl-3-octadecylimidazolium bromide	Melt processing / Compression moulding	100 µm	Oxygen	General engineering application

Reference	Particle	Matrix	Size before/after process	Chemical modification	Process	Film thickness	Molecular penetrant	Application
Mittal et al. [60]	Montmorillonite	Poly(propylene)	-	Dimethyldioctadecylammonium bromide	Melt processing / Compression moulding	100 µm	Oxygen	General engineering application
Monsivais-Barron et al. [149]	Montmorillonite	High density polyethylene	-	Dimethyl di(hydrogenated tallowalkyl) quaternary ammonium Quaternary ammonium salt Unmodified	Melt-compounding / Thermopressing	100 µm	Oxygen	Packaging application
Müller et al. [150]	Montmorillonite	Cassava starch	-	Methyl bis-2-hydroxyethyl tallow ammonium	Melt processing / Compression moulding	350 - 550 µm	Water vapor	General engineering
Nazarenko et al. [151]	Montmorillonite	Poly(styrene)	Thickness: 1nm Length: 80-300nm	Unmodified Octadecyldimethyl betaine Vinylbenzyldimethyldodecyl-ammonium chloride	Melt processing / Compression moulding	-	Oxygen	General engineering
Osman et al. [152]	Montmorillonite	Linear high density polyethylene	-	Octadecyltrimethyl ammonium chloride Dioctadecyldimethyl- ammonium bromide Methyltrioctadecyl ammonium bromide Tetraoctadecylammonium bromide	Melt processing / Compression moulding	60 µm	Oxygen	General engineering
Osman et al. [153]	Montmorillonite	Poly(propylene)	-	Octadecyltrimethyl ammonium Dimethyldioctaecyl ammonium Methyltrioctadecyl ammonium Benzylhexadecyldimethylammonium Docosyltriethylammonium	Melt processing / Compression moulding	100 µm	Oxygen	Packaging
Picard et al. [38]	Montmorillonite	Poly(amide 6)	-	Dihydroxy mthyl tallow quaterny ammonium	Melt processing / Compression moulding	75 - 85 µm	Oxygen / Water vapor	General engineering
Picard et al. [154]	Montmorillonite	Poly(lactic acid)	/ Aspect ratio 24	Dihydroxy mthyl tallow quaterny ammonium	Melt processing / Compression moulding	100 µm	Oxygen	General engineering
Ray et al. [146]	Montmorillonite	Poly(lactic acid)	-	Organically modified synthetic fluorine mica	Melt processing / Compression moulding	300 µm	Oxygen	Packaging
Rhim et al. [155]	Montmorillonite	Chitosan	-	Unmodified Dimethyl, hydrogenated tallow, 2-ethylhexyl quaterny ammonium	Solution / Casting	60 -70 µm	Water vapor	Packaging
Rhim et al.	Montmorillo	Poly(L-	-	Unmodified	Solution /	80 µm	Water vapor	Packaging

Reference	Particle	Matrix	Size before/after process	Chemical modification	Process	Film thickness	Molecular penetrant	Application
[36]	nite	lactide)		Dimethyl di(hydrogenated tallowalkyl) quaternary ammonium Bis-(2-hydrox-yethyl)methyl (hydrogenated tallowalkyl) quaternary ammonium	Casting			
Rhim et al. [36]	Montmorillonite	Food grade Agar	-		Solution / Casting	-	Water vapor	Packaging
Sanchez-Garcia et al. [42]	Montmorillonite	Blend (80%wt)PHB / (20%wt)PCL	-	Organophilic surface modified kaolinite	Melt processing / Compression moulding	100 - 700 µm	Oxygen	Packaging
Sanchez-Garcia et al. [34]	Montmorillonite	Poly(hydroxy butyrate-covalerate) Poly(e-caprolactone) Poly(lactic acid)	-	Organo-modification	Solution / Casting	100 µm	Oxygen / Water vapor	Packaging
Shah et al. [156]	Montmorillonite	Low density polyethylene Sodium ionomer of poly(ethylene-co-methacrylic acid)	-	Dimethyl di(hydrogenated tallow) ammonium	Melt processing / Blown processing	25.4 - 76.2µm	Oxygen / Carbon dioxide / Water vapor	Packaging
Slavutsky et al. [157]	Montmorillonite	Brea gum	-	Unmodified	Solution / Casting	-	Oxygen / Carbon dioxide / Water vapor	Packaging
Sothornvit et al. [158]	Montmorillonite	Whey protein	-	Unmodified Dimethyl di(hydrogenated tallowalkyl) quaternary ammonium Bis-(2-hydrox-yethyl)methyl (hydrogenated tallowalkyl) quaternary ammonium	Solution / Casting	150-190 µm	Water vapor	Packaging
Sothornvit et al. [159]	Montmorillonite	Whey protein	-	Bis-(2-hydrox-yethyl)methyl (hydrogenated tallowalkyl) quaternary ammonium	Solution / Casting	170 - 210 µm	Water vapor	Packaging
Strawhecker et al. [160]	Montmorillonite	Poly(vinyl alcohol)	-		Solution / Casting	89 µm	Water vapor	General engineering
Sun et al. [35]	α-zirconium phosphate	Epoxy resin	Thickness: 1nm Length: 100nm - 1µm	Polyoxyalkyleneamine Tetra-n-butyl ammonium hydroxide	Solution / Casting	1000 µm	Oxygen	General engineering
Swain et al. [161]	Boron nitride	Cellulose	70nm /		Solution / Thermopressing	5000 µm	Oxygen	Packaging
Rodriguez-	Montmorillo	Rice flour	-	Unmodified	Solution /	180 µm	Water vapor	Packaging

Reference	Particle	Matrix	Size before/after process	Chemical modification	Process	Film thickness	Molecular penetrant	Application
Marin et al. [162]	nite	Banana flour		Citric acid Citric acid / Sulphuric acid	Casting			
Tang et al. [163]	Montmorillonite	Corn starch Wheat starch Potato starch	-	Unmodified Onium ion modified MMT	Melt processing / Casting	-	Water vapor	Packaging
Thellen et al. [164]	Montmorillonite	Poly(L-lactide)	-	Dimethyl, hydrogenated tallow, 2-ethylhexyl quaterny ammonium	Melt processing / Blown processing	75 µm	Oxygen / Water vapor	Packaging
Tsai et al. [165]	Montmorillonite	Poly(methyl methacrylate)	/ Aspect ratio 100-150	Organo-modification	In situ free radical polymerization / casting	100 - 115 µm	Oxygen	Membrane
Tsai et al. [166]	Montmorillonite	Poly(methyl methacrylate)	-	Organo-modification	In situ polymerization / casting		Oxygen	Membrane
Tunc et al. [47]	Montmorillonite	Wheat gluten	Particle size distribution: 5-10µm	-	Solution - Casting	200 µm	Oxygen / Carbon dioxide / Water vapor	Packaging
Villaluenga et al. [167]	Montmorillonite	Isotactic polypropylene	-	Unmodified Octadecyl ammonium chloride	Melt processing / Compression moulding	100-170 µm	Oxygen	Membrane
Wang et al. [168]	Rectorite	Styrene butadiene rubber	/ Aspect ratio 20	Unmodified	Melt-compounding / Thermopressing	1000 µm	Oxygen	General engineering
Xu et al. [169]	Montmorillonite	Poly(urethane urea) segmented block copolymers	-	Octadecyl ammonium chloride	Solution / Casting	250 µm	Water vapor	General engineering
Yeh et al. [170]	Montmorillonite	Epoxy resin	-	Tetradecyltrimethylammonium chloride	Solution / Casting	250 µm	Oxygen / Water vapor	Membrane
Zehetmeyer et al. [171]	Montmorillonite	Poly(propylene)	-	Octadecyl ammonium chloride	Melt-compounding / Thermopressing	25 µm	Oxygen / Water vapor	Packaging
Zhang et al. [172]	Magnetic iron oxide Fe_3O_4	Zein	Long diagonal size: 200nm Height: 20nm /	Amphilic oleic acid	Solution / Casting	600 - 1300 µm	Oxygen / Water vapor	Packaging
Zhon et al. [173]	Montmorillonite	Ethylene vinyl acetate Low density polyethylene High density polyethylene	-	Dimethyl di(hydrogenated tallowalkyl) quaternary ammonium	Melt processing / Blown processing	-	Oxygen	General engineering

References:

[1] K. Petersen, P. Væggemose Nielsen, G. Bertelsen, M. Lawther, M.B. Olsen, N.H. Nilsson, et al., Potential of biobased materials for food packaging, Trends Food Sci. Technol. 10 (1999) 52–68. doi:10.1016/S0924-2244(99)00019-9.

[2] H. Angellier-coussy, V. Guillard, C. Guillaume, N. Gontard, Role of packaging in the smorgasbord of action for sustainable food consumption, Agro Food Ind. 23 (2013) 15–19.

[3] P.C. Lebaron, Z. Wang, T.J. Pinnavaia, Polymer-layered silicate nanocomposites: An overview, Appl. Clay Sci. 15 (1999) 11–29. doi:10.1016/S0169-1317(99)00017-4.

[4] M. Alexandre, P. Dubois, Polymer-layered silicate nanocomposites: preparation, properties and uses of a new class of materials, Mater. Sci. Eng. R Reports. 28 (2000) 1–63. doi:http://dx.doi.org/10.1016/S0927-796X(00)00012-7.

[5] T.S. Chung, L.Y. Jiang, Y. Li, S. Kulprathipanja, Mixed matrix membranes (MMMs) comprising organic polymers with dispersed inorganic fillers for gas separation, Prog. Polym. Sci. 32 (2007) 483–507. doi:10.1016/j.progpolymsci.2007.01.008.

[6] S. Pavlidou, C.D. Papaspyrides, A review on polymer-layered silicate nanocomposites, Prog. Polym. Sci. 33 (2008) 1119–1198. doi:10.1016/j.progpolymsci.2008.07.008.

[7] F. Chivrac, E. Pollet, L. Avérous, Progress in nano-biocomposites based on polysaccharides and nanoclays, Mater. Sci. Eng. R Reports. 67 (2009) 1–17. doi:10.1016/j.mser.2009.09.002.

[8] H. Cong, M. Radosz, B.F. Towler, Y. Shen, Polymer-inorganic nanocomposite membranes for gas separation, Sep. Purif. Technol. 55 (2007) 281–291. doi:10.1016/j.seppur.2006.12.017.

[9] V. Mittal, Polymer layered silicate nanocomposites: A review, Materials (Basel). 2 (2009) 992–1057. doi:10.3390/ma2030992.

[10] S. Sinha Ray, M. Okamoto, Polymer/layered silicate nanocomposites: A review from preparation to processing, Prog. Polym. Sci. 28 (2003) 1539–1641. doi:10.1016/j.progpolymsci.2003.08.002.

[11] S.S. Ray, M. Bousmina, Biodegradable polymers and their layered silicate nanocomposites: In greening the 21st century materials world, Prog. Mater. Sci. 50 (2005) 962–1079. doi:10.1016/j.pmatsci.2005.05.002.

[12] G. Choudalakis, a. D. Gotsis, Permeability of polymer/clay nanocomposites: A review, Eur. Polym. J. 45 (2009) 967–984. doi:10.1016/j.eurpolymj.2009.01.027.

[13] A.M. Youssef, Polymer Nanocomposites as a New Trend for Packaging Applications, Polym. Plast. Technol. Eng. 52 (2013) 635–660. doi:10.1080/03602559.2012.762673.

[14] D.R. Paul, L.M. Robeson, Polymer nanotechnology: Nanocomposites, Polymer (Guildf). 49 (2008) 3187–3204. doi:10.1016/j.polymer.2008.04.017.

[15] A. Arora, G.W. Padua, Review: Nanocomposites in food packaging, J. Food Sci. 75 (2010) 43–49. doi:10.1111/j.1750-3841.2009.01456.x.

[16] C. Silvestre, D. Duraccio, S. Cimmino, Food packaging based on polymer nanomaterials, Prog. Polym. Sci. 36 (2011) 1766–1782. doi:10.1016/j.progpolymsci.2011.02.003.

[17] J.-W. Rhim, H.-M. Park, C.-S. Ha, Bio-nanocomposites for food packaging applications, Prog. Polym. Sci. 38 (2013) 1629–1652. doi:10.1016/j.progpolymsci.2013.05.008.

[18] H.M.C. De Azeredo, Nanocomposites for food packaging applications, Food Res. Int. 42 (2009) 1240–1253. doi:10.1016/j.foodres.2009.03.019.

[19] Y. Cui, S. Kumar, B. Rao Kona, D. van Houcke, Gas barrier properties of polymer/clay nanocomposites, RSC Adv. 5 (2015) 63669–63690. doi:10.1039/C5RA10333A.

[20] P. Buche, J. Dibie, M. Ibanescu, L. Soler, Fuzzy web data tables integration guided by an ontological and terminological resource, in: IEEE Trans. Knowl. Data Eng., Institute of Electrical and Electronics Engineers (IEEE), 2011: p. PP (99), p.1.

[21] S.P. Koenig, L. Wang, J. Pellegrino, J.S. Bunch, Selective molecular sieving through porous graphene, Nat. Nanotechnol. 7 (2012) 728. http://dx.doi.org/10.1038/nnano.2012.162.

[22] B. Tan, N.L. Thomas, A review of the water barrier properties of polymer/clay and polymer/graphene nanocomposites, J. Memb. Sci. 514 (2016) 595–612. doi:10.1016/j.memsci.2016.05.026.

[23] Y. Cui, S.I. Kundalwal, S. Kumar, Gas barrier performance of graphene/polymer nanocomposites, Carbon N. Y. 98 (2016) 313–333. doi:10.1016/j.carbon.2015.11.018.

[24] N. Saheb, J. Jog, Natural Fiber Polymer Composites : A Review, Adv. Polym. Technol. 2329 (2015) 351–363. doi:10.1002/(SICI)1098-2329(199924)18.

[25] G. Siqueira, J. Bras, A. Dufresne, Cellulosic bionanocomposites: A review of preparation, properties and applications, Polymers (Basel). 2 (2010) 728–765. doi:10.3390/polym2040728.

[26] J.C. Maxwell, A Treatise on Electricity and Magnetism, Oxford University Press, London, 1873.

[27] O.H. Wiener, Die Theorie des Mischkörpers für das Feld der stationären Strömung. 1 Die Mittelwertsätze für Kraft, Polarisation und Energie, B.G. Teubner, Leipzig, 1912.

[28] L.E. Nielsen, Models for the permeability of filled polymer systems, J. Macromol. Sci. Part A- Chem. 1 (1967) 929–942.

[29] K.G. Papadokostaki, M. Minelli, F. Doghieri, J.H. Petropoulos, A fundamental study of the extent of meaningful application of Maxwell's and Wiener's equations to the permeability of binary composite materials. Part II: A useful explicit analytical approach, Chem. Eng. Sci. 131 (2015) 353–359. doi:10.1016/j.ces.2015.03.031.

[30] K.G. Gatos, J. Karger-Kocsis, Effect of the aspect ratio of silicate platelets on the mechanical and barrier properties of hydrogenated acrylonitrile butadiene rubber (HNBR)/layered silicate nanocomposites, Eur. Polym. J. 43 (2007) 1097–1104. doi:10.1016/j.eurpolymj.2007.01.032.

[31] H. Angellier-Coussy, E. Gastaldi, F.C. Da Silva, N. Gontard, V. Guillard, Nanoparticle size and water diffusivity in nanocomposite agro-polymer based films, Eur. Polym. J. 49 (2013) 299–306. doi:10.1016/j.eurpolymj.2012.11.006.

[32] T.D. Fornes, D.R. Paul, Modeling properties of nylon 6/clay nanocomposites using composite theories, Polymer (Guildf). 44 (2003) 4993–5013. doi:10.1016/S0032-3861(03)00471-3.

[33] H.C. Koh, J.S. Park, M.A. Jeong, H.Y. Hwang, Y.T. Hong, S.Y. Ha, et al., Preparation and gas permeation properties of biodegradable polymer/layered silicate nanocomposite membranes, Desalination. 233 (2008) 201–209. doi:10.1016/j.desal.2007.09.043.

[34] M.D. Sanchez-Garcia, E. Gimenez, J.M. Lagaron, Morphology and barrier properties of solvent cast composites of thermoplastic biopolymers and purified cellulose fibers, Carbohydr. Polym. 71 (2008) 235–244. doi:10.1016/j.carbpol.2007.05.041.

[35] L. Sun, W.J. Boo, A. Clearfield, H.J. Sue, H.Q. Pham, Barrier properties of model epoxy nanocomposites, J. Memb. Sci. 318 (2008) 129–136. doi:10.1016/j.memsci.2008.02.041.

[36] J.W. Rhim, Effect of clay contents on mechanical and water vapor barrier properties of agar-based nanocomposite films, Carbohydr. Polym. 86 (2011) 691–699. doi:10.1016/j.carbpol.2011.05.010.

[37] R.K. Bharadwaj, A.R. Mehrabi, C. Hamilton, C. Trujillo, M. Murga, Structure-property relationships in cross-linked polyester -clay nanocomposites, Polymer (Guildf). 43 (2002) 3699–3705. doi:https://doi.org/10.1016/S0032-3861(02)00187-8.

[38] E. Picard, A. Vermogen, J.F. Gérard, E. Espuche, Barrier properties of nylon 6-montmorillonite nanocomposite membranes prepared by melt blending: Influence of the clay content and

dispersion state. Consequences on modelling, J. Memb. Sci. 292 (2007) 133–144. doi:10.1016/j.memsci.2007.01.030.

[39] J.-H. Chang, K.M. Park, D. Cho, H.S. Yang, K.J. Ihn, Preparation and characterization of polyimide / organoclay nanocomposites, Polym. Eng. Sci. 41 (2001) 1514–1520.

[40] A. Zhu, A. Cai, J. Zhang, H. Jia, J. Wang, PMMA- grafted -Silica / PVC Nanocomposites : Mechanical Performance and Barrier Properties, J. Appl. Polym. Sci. 108 (2008) 2189–2196. doi:10.1002/app.

[41] P.B. Messersmith, Synthesis and Barrier Properties of Poly (e-Capro1actone) - Layered Silicate Nanocomposites, J. Polym. Sci. Part A Polym. Chem. 33 (1995) 1047–1057.

[42] M.D. Sanchez-Garcia, E. Gimenez, J.M. Lagaron, Morphology and Barrier Properties of Nanobiocomposites of Poly (3-hydroxybutyrate) and Layered Silicates, J. Appl. Polym. Sci. 108 (2008) 2787–2801. doi:10.1002/app.

[43] M. Sadeghi, M. Mehdi Talakesh, B. Ghalei, M. Shafiei, Preparation, characterization and gas permeation properties of a polycaprolactone based polyurethane-silica nanocomposite membrane, J. Memb. Sci. 427 (2013) 21–29. doi:10.1016/j.memsci.2012.07.036.

[44] V. Vladimirov, C. Betchev, A. Vassiliou, G. Papageorgiou, D. Bikiaris, Dynamic mechanical and morphological studies of isotactic polypropylene/fumed silica nanocomposites with enhanced gas barrier properties, Compos. Sci. Technol. 66 (2006) 2935–2944. doi:10.1016/j.compscitech.2006.02.010.

[45] A. Vassiliou, D. Bikiaris, E. Pavlidou, Optimizing Melt-Processing Conditions for the Preparation of iPP/Fumed Silica Nanocomposites: Morphology, Mechanical and Gas Permeability Properties, Macromol. React. Eng. 1 (2007) 488–501. doi:10.1002/mren.200700006.

[46] H. Ghasemi, P.J. Carreau, M.R. Kamal, S.H. Tabatabaei, Properties of PET/Clay Nanocomposte films, Polym. Eng. Sci. 52 (2012) 420–430. doi:10.1002/pen.

[47] S. Tunc, H. Angellier, Y. Cahyana, P. Chalier, N. Gontard, E. Gastaldi, Functional properties of wheat gluten/montmorillonite nanocomposite films processed by casting, J. Memb. Sci. 289 (2007) 159–168. doi:10.1016/j.memsci.2006.11.050.

[48] J.-E. Lee, K.M. Kim, Characteristics of Soy Protein Isolate-Montmorillonite Composite Films Jung-Eun, J. Appl. Polym. Sci. 118 (2010) 2257–2263. doi:10.1002/app.

[49] C.J. Cornelius, E. Marand, Hybrid silica-polyimide composite membranes: gas transport properties, J. Memb. Sci. 202 (2002) 97–118. doi:10.1016/S0376-7388(01)00734-7.

[50] R.A. Zoppi, S. Neves, S.P. Nunes, Hybrid films of poly (ethylene oxide- b -amide-6) containing sol – gel silicon or titanium oxide as inorganic fillers : effect of morphology and mechanical properties on gas permeability, Polymer (Guildf). 41 (2000) 5461–5470.

[51] C. Bilbao-Sainz, J. Bras, T. Williams, T. Sénechal, W. Orts, HPMC reinforced with different cellulose nano-particles, Carbohydr. Polym. 86 (2011) 1549–1557. doi:10.1016/j.carbpol.2011.06.060.

[52] A.F. Ismail, N.H. Rahim, A. Mustafa, T. Matsuura, B.C. Ng, S. Abdullah, et al., Gas separation performance of polyethersulfone / multi-walled carbon nanotubes mixed matrix membranes, 80 (2011) 20–31. doi:10.1016/j.seppur.2011.03.031.

[53] S. Rafiq, Z. Man, A. Maulud, N. Muhammad, S. Maitra, Separation of CO 2 from CH 4 using polysulfone/ polyimide silica nanocomposite membranes, Sep. Purif. Technol. 90 (2012) 162–172. doi:10.1016/j.seppur.2012.02.031.

[54] C.Y. Liang, P. Uchytil, R. Petrychkovych, Y.C. Lai, K. Friess, M. Sipek, et al., A comparison on gas separation between PES (polyethersulfone)/MMT (Na-montmorillonite) and PES/TiO 2 mixed matrix membranes, in: Sep. Purif. Technol., Elsevier B.V., 2012: pp. 57–63.

doi:10.1016/j.seppur.2012.03.016.

[55] S. Matteucci, V.A. Kusuma, D. Sanders, S. Swinnea, B.D. Freeman, Gas transport in TiO2 nanoparticle-filled poly(1-trimethylsilyl-1-propyne), J. Memb. Sci. 307 (2008) 196–217. doi:10.1016/j.memsci.2007.09.035.

[56] F. Moghadam, M.R. Omidkhah, E. Vasheghani-Farahani, M.Z. Pedram, F. Dorosti, The effect of TiO2 nanoparticles on gas transport properties of Matrimid5218-based mixed matrix membranes, Sep. Purif. Technol. 77 (2011) 128–136. doi:10.1016/j.seppur.2010.11.032.

[57] V.N. Dougnac, R. Alamillo, B.C. Peoples, R. Quijada, Effect of particle diameter on the permeability of polypropylene/SiO2 nanocomposites, Polymer (Guildf). 51 (2010) 2918–2926. doi:10.1016/j.polymer.2010.02.014.

[58] A.I. Romero, M.L. Parentis, A.C. Habert, E.E. Gonzo, Synthesis of polyetherimide/silica hybrid membranes by the sol-gel process: Influence of the reaction conditions on the membrane properties, J. Mater. Sci. 46 (2011) 4701–4709. doi:10.1007/s10853-011-5380-4.

[59] R. Surya Murali, S. Sridhar, T. Sankarshana, Y.V.L. Ravikumar, Gas permeation behavior of pebax-1657 nanocomposite membrane incorporated with multiwalled carbon nanotubes, Ind. Eng. Chem. Res. 49 (2010) 6530–6538. doi:10.1021/ie9016495.

[60] V. Mittal, Gas permeation and mechanical properties of polypropylene nanocomposites with thermally-stable imidazolium modified clay, Eur. Polym. J. 43 (2007) 3727–3736. doi:10.1016/j.eurpolymj.2007.06.015.

[61] D. Bracho, V.N. Dougnac, H. Palza, R. Quijada, Functionalization of silica nanoparticles for polypropylene nanocomposite applications, J. Nanomater. 2012 (2012). doi:10.1155/2012/263915.

[62] N. Dogan, T.H. McHugh, Effects of microcrystalline cellulose on functional properties of hydroxy propyl methyl cellulose microcomposite films., J. Food Sci. 72 (2007). doi:10.1111/j.1750-3841.2006.00237.x.

[63] J. Chang, Y.U. An, G.S. Sur, Poly(Lactic Acid) Nanocomposites with Various Organoclays. I.Thermomechanical Properties, Morphology, and Gas Permeability, J. Polym. Sci. Part B Polym. Phys. 41 (2003) 94–103. doi:10.1002/polb.10349.

[64] M. Iwata, T. Adachi, M. Tomidokoro, M. Ohta, T. Kobayashi, Hybrid Sol – Gel Membranes of Polyacrylonitrile – Tetraethoxysilane Composites for Gas Permselectivity, (2002).

[65] A. Saxena, A.J. Ragauskas, Water transmission barrier properties of biodegradable films based on cellulosic whiskers and xylan, Carbohydr. Polym. 78 (2009) 357–360. doi:10.1016/j.carbpol.2009.03.039.

[66] S.A. Paralikar, J. Simonsen, J. Lombardi, Poly(vinyl alcohol)/cellulose nanocrystal barrier membranes, J. Memb. Sci. 320 (2008) 248–258. doi:10.1016/j.memsci.2008.04.009.

[67] D.J. Chaiko, A.A. Leyva, Thermal transitions and barrier properties of olefinic nanocomposites, Chem. Mater. 17 (2005) 13–19. doi:10.1021/cm0302680.

[68] N. Follain, S. Belbekhouche, J. Bras, G. Siqueira, S. Marais, A. Dufresne, Water transport properties of bio-nanocomposites reinforced by Luffa cylindrica cellulose nanocrystals, J. Memb. Sci. 427 (2013) 218–229. doi:10.1016/j.memsci.2012.09.048.

[69] S. Takahashi, D.R. Paul, Gas permeation in poly (ether imide) nanocomposite membranes based on surface-treated silica . Part 2 : With chemical coupling to matrix, Polymer (Guildf). 47 (2006) 7535–7547. doi:10.1016/j.polymer.2006.08.036.

[70] J.H. Kim, Y.M. Lee, Gas permeation properties of poly (amide-6-b-ethylene oxide)– silica hybrid membranes, Membr. Sci. 193 (2001) 209–225.

[71] H. Cong, X. Hu, M. Radosz, Y. Shen, Brominated Poly (2 , 6-diphenyl-1 , 4-phenylene oxide) and Its Silica Nanocomposite Membranes for Gas Separation Brominated Poly (2 , 6-diphenyl-1 , 4-phenylene oxide) and Its Silica Nanocomposite Membranes for Gas Separation, (2007) 2567–2575. doi:10.1021/ie061494x.

[72] M. Sadeghi, M.A. Semsarzadeh, H. Moadel, Enhancement of the gas separation properties of polybenzimidazole (PBI) membrane by incorporation of silica nano particles, J. Memb. Sci. 331 (2009) 21–30. doi:10.1016/j.memsci.2008.12.073.

[73] T. Suzuki, Y. Yamada, Physical and Gas Transport Properties of Novel Hyperbranched Polyimide ? Silica Hybrid Membranes, Polym. Bull. 53 (2004) 139–146. doi:10.1007/s00289-004-0322-9.

[74] M. Sadeghi, G. Khanbabaei, A.H.S. Dehaghani, M. Sadeghi, M.A. Aravand, M. Akbarzade, et al., Gas permeation properties of ethylene vinyl acetate–silica nanocomposite membranes, J. Memb. Sci. 322 (2008) 423–428. doi:10.1016/j.memsci.2008.05.077.

[75] T. Kono, Y. Hu, T. Masuda, K. Tanaka, R.D. Priestley, B.D. Freeman, Effect of Fumed Silica Nanoparticles on the Gas Permeation Properties of Substituted Polyacetylene Membranes, Polym. Bull. 58 (2007) 995–1003. doi:10.1007/s00289-006-0720-2.

[76] J. Ahn, W.J. Chung, I. Pinnau, M.D. Guiver, Polysulfone/silica nanoparticle mixed-matrix membranes for gas separation, J. Memb. Sci. 314 (2008) 123–133. doi:10.1016/j.memsci.2008.01.031.

[77] E. Jacquelot, E. Espuche, J.F. Gérard, J. Duchet, P. Mazabraud, Morphology and gas barrier properties of polyethylene-based nanocomposites, J. Polym. Sci. Part B Polym. Phys. 44 (2006) 431–440. doi:10.1002/polb.20707.

[78] D. Merinska, H. Kubisova, A. Kalendova, P. Svoboda, J. Hromadkova, Processing and Properties of Polyethylene/Montmorillonite Nanocomposites, J. Thermoplast. Compos. Mater. 25 (2011) 115–131. doi:10.1177/0892705711404939.

[79] A.P. Meera, S. Thomas P., S. Thomas, Effect of organoclay on the gas barrier properties of natural rubber nanocomposites, Polym. Compos. 33 (2012) 524–531. doi:10.1002/pc.22188.

[80] K. Alena, M. Dagmar, G.J. Francois, S. Miroslav, Polymer/clay nanocomposites and their gas barrier properties, Polym. Compos. 34 (2013) 1418–1424. doi:10.1002/pc.22541.

[81] M. Sadeghi, M.A. Semsarzadeh, M. Barikani, M. Pourafshari Chenar, Gas separation properties of polyether-based polyurethane-silica nanocomposite membranes, J. Memb. Sci. 376 (2011) 188–195. doi:10.1016/j.memsci.2011.04.021.

[82] M.A. Semsarzadeh, B. Ghalei, Preparation, Characterization and gas permeation properties of polyurethane-silica/polyvinyl alcohol mixed matrix membranes, J. Memb. Sci. 432 (2013) 115–125. doi:10.1016/j.memsci.2013.01.005.

[83] J. Ahn, W.J. Chung, I. Pinnau, J. Song, N. Du, G.P. Robertson, et al., Gas transport behavior of mixed-matrix membranes composed of silica nanoparticles in a polymer of intrinsic microporosity (PIM-1), J. Memb. Sci. 346 (2010) 280–287. doi:10.1016/j.memsci.2009.09.047.

[84] Q. Hu, E. Marand, S. Dhingra, D. Fritsch, J. Wen, Poly (amide-imide)/ TiO2 nano-composite gas separation membranes " Fabrication and characterization, J. Memb. Sci. 135 (1997) 65–79. doi:http://dx.doi.org/10.1016/S0376-7388(97)00120-8.

[85] C. Joly, M. Smaihi, L. Porcar, R.D. Noble, Polyimide−Silica Composite Materials: How Does Silica Influence Their Microstructure and Gas Permeation Properties?, Chem. Mater. 11 (1999) 2331–2338. doi:10.1021/cm9805018.

[86] S. Kim, E. Marand, High permeability nano-composite membranes based on mesoporous MCM-41 nanoparticles in a polysulfone matrix, Microporous Mesoporous Mater. 114 (2008) 129–136.

doi:10.1016/j.micromeso.2007.12.028.

[87] Y. Kong, H. Du, J. Yang, D. Shi, Y. Wang, Study on polyimide / TiO , nanocomposite membranes for gas separation, Desalination. 146 (2002) 49–55.

[88] S. Matteucci, V.A. Kusuma, S. Swinnea, B.D. Freeman, Gas permeability, solubility and diffusivity in 1,2-polybutadiene containing brookite nanoparticles, Polymer (Guildf). 49 (2008) 757–773. doi:10.1016/j.polymer.2007.12.011.

[89] N.P. Patel, A.C. Miller, R.J. Spontak, Highly CO2-permeable and selective polymer nanocomposite membranes, Adv. Mater. 15 (2003) 729–733. doi:10.1002/adma.200304712.

[90] N.P. Patel, A.C. Miller, R.J. Spontak, Highly CO2-permeable and -selective membranes derived from crosslinked poly(ethylene glycol) and its nanocomposites, Adv. Funct. Mater. 14 (2004) 699–707. doi:10.1002/adfm.200305136.

[91] S. Ulutan, D. Balköse, Diffusivity, solubility and permeability of water vapor in flexible PVC/silica composite membranes, J. Memb. Sci. 115 (1996) 217–224. doi:10.1016/0376-7388(96)00030-0.

[92] X. Yu, Z. Wang, J. Zhao, F. Yuan, S. Li, J. Wang, et al., An effective method to improve the performance of fixed carrier membrane via incorporation of CO2-selective adsorptive silica nanoparticles, in: Chinese J. Chem. Eng., Chemical Industry and Engineering Society of China (CIESC) and Chemical Industry Press (CIP), 2011: pp. 821–832. doi:10.1016/S1004-9541(11)60062-1.

[93] J.J. Zhou, S.Y. Wang, S. Gunasekaran, Preparation and characterization of whey protein film incorporated with TiO2 nanoparticles, J. Food Sci. 74 (2009). doi:10.1111/j.1750-3841.2009.01270.x.

[94] H.M.C. Azeredo, L.H.C. Mattoso, D. Wood, T.G. Williams, R.J. Avena-Bustillos, T.H. McHugh, Nanocomposite edible films from mango puree reinforced with cellulose nanofibers, J. Food Sci. 74 (2009) 31–35. doi:10.1111/j.1750-3841.2009.01186.x.

[95] H.M.C. Azeredo, L.H.C. Mattoso, R.J. Avena-Bustillos, G.C. Filho, M.L. Munford, D. Wood, et al., Nanocellulose reinforced chitosan composite films as affected by nanofiller loading and plasticizer content, J. Food Sci. 75 (2010) 1–7. doi:10.1111/j.1750-3841.2009.01386.x.

[96] P.R. Chang, R. Jian, P. Zheng, J. Yu, X. Ma, Preparation and properties of glycerol plasticized-starch (GPS)/cellulose nanoparticle (CN) composites, Carbohydr. Polym. 79 (2010) 301–305. doi:10.1016/j.carbpol.2009.08.007.

[97] H. Cong, J. Zhang, M. Radosz, Y. Shen, Carbon nanotube composite membranes of brominated poly(2,6-diphenyl-1,4-phenylene oxide) for gas separation, J. Memb. Sci. 294 (2007) 178–185. doi:10.1016/j.memsci.2007.02.035.

[98] E. Espino-Pérez, J. Bras, V. Ducruet, A. Guinault, A. Dufresne, S. Domenek, Influence of chemical surface modification of cellulose nanowhiskers on thermal, mechanical, and barrier properties of poly(lactide) based bionanocomposites, Eur. Polym. J. 49 (2013) 3144–3154. doi:10.1016/j.eurpolymj.2013.07.017.

[99] J. George, Siddaramaiah, High performance edible nanocomposite films containing bacterial cellulose nanocrystals, Carbohydr. Polym. 87 (2012) 2031–2037. doi:10.1016/j.carbpol.2011.10.019.

[100] S. Kim, T.W. Pechar, E. Marand, Poly(imide siloxane) and carbon nanotube mixed matrix membranes for gas separation, Desalination. 192 (2006) 330–339. doi:10.1016/j.desal.2005.03.098.

[101] S. Kim, L. Chen, J.K. Johnson, E. Marand, Polysulfone and functionalized carbon nanotube mixed matrix membranes for gas separation: Theory and experiment, J. Memb. Sci. 294 (2007) 147–158. doi:10.1016/j.memsci.2007.02.028.

[102] S. Mondal, J.L. Hu, Microstructure and Water Vapor Transport Properties of Functionalized Carbon

Nanotube-Reinforced Dense- Segmented Polyurethane Composite Membranes, Polym. Eng. Sci. 48 (2008) 1718–1724. doi:10.1002/pen.

[103] R. Pantani, G. Gorrasi, G. Vigliotta, M. Murariu, P. Dubois, PLA-ZnO nanocomposite films: Water vapor barrier properties and specific end-use characteristics, Eur. Polym. J. 49 (2013) 3471–3482. doi:10.1016/j.eurpolymj.2013.08.005.

[104] A.K. Pradhan, S.K. Swain, Electrical conductivity and oxygen permeability of polyacrylonitrile/ multiwalled carbon nanotubes composites, Polym. Compos. 33 (2012) 1114–1119. doi:10.1002/pc.22239.

[105] M.D. Sanchez-Garcia, J.M. Lagaron, S. V Hoa, Effect of addition of carbon nanofibers and carbon nanotubes on properties of thermoplastic biopolymers, Compos. Sci. Technol. 70 (2010) 1095–1105. doi:10.1016/j.compscitech.2010.02.015.

[106] M.D. Sanchez-Garcia, J.M. Lagaron, On the use of plant cellulose nanowhiskers to enhance the barrier properties of polylactic acid, Cellulose. 17 (2010) 987–1004. doi:10.1007/s10570-010-9430-x.

[107] M.D. Sánchez-García, L. Hilliou, J.M. Lagarón, Morphology and water barrier properties of nanobiocomposites of κ/l-hybrid carrageenan and cellulose nanowhiskers, J. Agric. Food Chem. 58 (2010) 12847–12857. doi:10.1021/jf102764e.

[108] J. Yu, J. Yang, B. Liu, X. Ma, Preparation and characterization of glycerol plasticized-pea starch/ZnO-carboxymethylcellulose sodium nanocomposites, Bioresour. Technol. 100 (2009) 2832–2841. doi:10.1016/j.biortech.2008.12.045.

[109] M. Abdollahi, M. Alboofetileh, M. Rezaei, R. Behrooz, Comparing physico-mechanical and thermal properties of alginate nanocomposite films reinforced with organic and/or inorganic nanofillers, Food Hydrocoll. 32 (2013) 416–424. doi:10.1016/j.foodhyd.2013.02.006.

[110] M. Alboofetileh, M. Rezaei, H. Hosseini, M. Abdollahi, Effect of montmorillonite clay and biopolymer concentration on the physical and mechanical properties of alginate nanocomposite films, J. Food Eng. 117 (2013) 26–33. doi:10.1016/j.jfoodeng.2013.01.042.

[111] B. Alexandre, L. Colasse, D. Langevin, P. Médéric, T. Aubry, C. Chappey, et al., Transport mechanisms of small molecules through polyamide 12/montmorillonite nanocomposites., J. Phys. Chem. B. 114 (2010) 8827–37. doi:10.1021/jp911666b.

[112] S.S. Ali, X. Tang, S. Alavi, J. Faubion, Structure and Physical Properties of Starch / Poly Vinyl Alcohol / Sodium Montmorillonite Nanocomposite Films, (2011) 12384–12395.

[113] H. Angellier, S. Molina-Boisseau, A. Dufresne, Mechanical properties of waxy maize starch nanocrystal reinforced natural rubber, Macromolecules. 38 (2005) 9161–9170. doi:10.1021/ma0512399.

[114] H.J. Bae, H.J. Park, S.I. Hong, Y.J. Byun, D.O. Darby, R.M. Kimmel, et al., Effect of clay content, homogenization RPM, pH, and ultrasonication on mechanical and barrier properties of fish gelatin/montmorillonite nanocomposite films, LWT - Food Sci. Technol. 42 (2009) 1179–1186. doi:10.1016/j.lwt.2008.12.016.

[115] M. Balachandran, S.S. Bhagawan, Mechanical , thermal and transport properties of nitrile rubber (NBR) — nanoclay composites, J. Polym. Res. 19 (2012) 9809. doi:10.1007/s10965-011-9809-x.

[116] A.T. Chien, K.F. Lin, Morphology and permeability of exfoliated PVAc-MMT nanocomposite films cast from soap-free emulsion-polymerized latices, J. Polym. Sci. Part A Polym. Chem. 45 (2007) 5583–5589. doi:10.1002/pola.22304.

[117] F. Chivrac, H. Angellier-Coussy, V. Guillard, E. Pollet, L. Avérous, How does water diffuse in

starch/montmorillonite nano-biocomposite materials?, Carbohydr. Polym. 82 (2010) 128–135. doi:10.1016/j.carbpol.2010.04.036.

[118] W.J. Choi, S.H. Kim, Y. Jin Kim, S.C. Kim, Synthesis of chain-extended organifier and properties of polyurethane/clay nanocomposites, Polymer (Guildf). 45 (2004) 6045–6057. doi:10.1016/j.polymer.2004.06.033.

[119] R.N. Choi, C.I. Cheigh, S.Y. Lee, M.S. Chung, Preparation and Properties of Polypropylene/Clay Nanocomposites for Food Packaging, J. Food Sci. 76 (2011) 62–67. doi:10.1111/j.1750-3841.2011.02351.x.

[120] S. Dash, S.K. Swain, Synthesis of thermal and chemical resistant oxygen barrier starch with reinforcement of nano silicon carbide, Carbohydr. Polym. 97 (2013) 758–763. doi:10.1016/j.carbpol.2013.05.061.

[121] Z. Duan, N.L. Thomas, W. Huang, Water vapour permeability of poly(lactic acid) nanocomposites, J. Memb. Sci. 445 (2013) 112–118. doi:10.1016/j.memsci.2013.06.008.

[122] E. Dunkerley, D. Schmidt, Effects of Composition , Orientation and Temperature on the O 2 Permeability of Model Polymer / Clay Nanocomposites, (2010) 10536–10544. doi:10.1021/ma1018846.

[123] I. Echeverría, P. Eisenberg, A.N. Mauri, Nanocomposites films based on soy proteins and montmorillonite processed by casting, J. Memb. Sci. 449 (2014) 15–26. doi:10.1016/j.memsci.2013.08.006.

[124] M. Fasihi, M.R. Abolghasemi, Oxygen Barrier and Mechanical Properties of Masterbatch- Based PA6 / Nanoclay Composite Films, J. Appl. Polym. Sci. 125 (2011) E2–E8. doi:10.1002/app.

[125] E. Fortunati, M. Peltzer, I. Armentano, L. Torre, a Jiménez, J.M. Kenny, Effects of modified cellulose nanocrystals on the barrier and migration properties of PLA nano-biocomposites., Carbohydr. Polym. 90 (2012) 948–56. doi:10.1016/j.carbpol.2012.06.025.

[126] O. Gain, E. Espuche, E. Pollet, M. Alexandre, P. Dubois, Gas barrier properties of poly(ε-caprolactone)/clay nanocomposites: Influence of the morphology and polymer/clay interactions, J. Polym. Sci. Part B Polym. Phys. 43 (2005) 205–214. doi:10.1002/polb.20316.

[127] C. Guo, L. Zhou, J. Lv, Effects of expandable graphite and modified ammonium polyphosphate on the flame-retardant and mechanical properties of wood flour-polypropylene composites, Polym. Polym. Compos. 21 (2013) 449–456. doi:10.1002/app.

[128] J.M. Herrera-alonso, Z. Sedlakova, E. Marand, Gas barrier properties of nanocomposites based on in situ polymerized poly (n -butyl methacrylate) in the presence of surface modified montmorillonite, J. Memb. Sci. 349 (2010) 251–257. doi:10.1016/j.memsci.2009.11.057.

[129] F. Horst, W. Tuckart, L. Del Blanco, M.D. Failla, L.M. Quinzani, Effect of Clay Concentration on the Wear Behavior and Permeability of Polypropylene / Clay Nanocomposites, J. Appl. Polym. Sci. 125 (2012) 495–502. doi:10.1002/app.

[130] S. Hotta, D.R. Paul, Nanocomposites formed from linear low density polyethylene and organoclays, Polymer (Guildf). 45 (2004) 7639–7654. doi:10.1016/j.polymer.2004.08.059.

[131] C. Huang, G. Jang, K. Chang, W. Hung, J. Yeh, High-performance polyimide – clay nanocomposite materials based on a dual intercalating agent system, Polym. Int. 57 (2008) 605–611. doi:10.1002/pi.

[132] M. Ito, K. Nagai, Thermal Aging and Oxygen Permeation of Nylon-6 and Nylon-6 / Montmorillonite Composites, (2010) 1–8. doi:10.1002/app.

[133] Y. Kasirga, A. Oral, C. Caner, Preparation and Characterization of Chitosan/ Montmorillonite-K10

Nanocomposites Films for Food Packaging Applications, Polym. Compos. 33 (2012) 1874–1882. doi:DOI 10.1002/pc.22310 Published.

[134] V. Katiyar, N. Gerds, C.B. Koch, J. Risbo, H.C.B. Hansen, D. Plackett, Melt Processing of Poly (L -Lactic Acid) in the Presence of Organomodified Anionic or Cationic Clays, J. Appl. Polym. Sci. 122 (2011) 112–125. doi:10.1002/app.

[135] Z. Ke, B. Yongping, Improve the gas barrier property of PET film with montmorillonite by in situ interlayer polymerization, Mater. Lett. 59 (2005) 3348–3351. doi:10.1016/j.matlet.2005.05.070.

[136] S.K. Kisku, S.K. Swain, Synthesis and characterization of Chitosan/Boron nitride composites, in: J. Am. Ceram. Soc., 2012: pp. 2753–2757. doi:10.1111/j.1551-2916.2012.05140.x.

[137] S.K. Kisku, S. Dash, S.K. Swain, Dispersion of SiC nanoparticles in cellulose for study of tensile, thermal and oxygen barrier properties, Carbohydr. Polym. 99 (2014) 306–310. doi:10.1016/j.carbpol.2013.08.035.

[138] J.K. Kim, C. Hu, R.S.C. Woo, M.L. Sham, Moisture barrier characteristics of organoclay-epoxy nanocomposites, Compos. Sci. Technol. 65 (2005) 805–813. doi:10.1016/j.compscitech.2004.10.014.

[139] E. Kristo, C.G. Biliaderis, Physical properties of starch nanocrystal-reinforced pullulan films, Carbohydr. Polym. 68 (2007) 146–158. doi:10.1016/j.carbpol.2006.07.021.

[140] P. Kumar, K.P. Sandeep, S. Alavi, V.D. Truong, R.E. Gorga, Effect of Type and Content of Modified Montmorillonite on the Structure and Properties of Bio-Nanocomposite Films Based on Soy Protein Isolate and Montmorillonite, J. Food Sci. 75 (2010) 46–56. doi:10.1111/j.1750-3841.2010.01633.x.

[141] P. Kumar, K.P. Sandeep, S. Alavi, V.D. Truong, R.E. Gorga, Preparation and characterization of bio-nanocomposite films based on soy protein isolate and montmorillonite using melt extrusion, J. Food Eng. 100 (2010) 480–489. doi:10.1016/j.jfoodeng.2010.04.035.

[142] T. Lan, P.D. Kaviratna, T.J. Pinnavaia, On the Nature of Polyumide-Clay hibrid composites, Chem. Mater. 6 (1994) 573–575.

[143] M. Lavorgna, F. Piscitelli, P. Mangiacapra, G.G. Buonocore, Study of the combined effect of both clay and glycerol plasticizer on the properties of chitosan films, Carbohydr. Polym. 82 (2010) 291–298. doi:10.1016/j.carbpol.2010.04.054.

[144] J.H. Lee, D. Jung, C.E. Hong, K.Y. Rhee, S.G. Advani, Properties of polyethylene-layered silicate nanocomposites prepared by melt intercalation with a PP-g-MA compatibilizer, Compos. Sci. Technol. 65 (2005) 1996–2002. doi:10.1016/j.compscitech.2005.03.015.

[145] C.H. Lee, A.T. Chien, M.H. Yen, K.F. Lin, Poly(methyl acrylate-co-methyl methacrylate)/montmorillonite nanocomposites fabricated by soap-free emulsion polymerization, J. Polym. Res. 15 (2008) 331–336. doi:10.1007/s10965-008-9175-5.

[146] J. Luecha, N. Sozer, J.L. Kokini, Synthesis and properties of corn zein/montmorillonite nanocomposite films, J. Mater. Sci. 45 (2010) 3529–3537. doi:10.1007/s10853-010-4395-6.

[147] C. Masclaux, F. Gouanve, E. Espuche, Experimental and modelling studies of transport in starch nanocomposite films as affected by relative humidity, J. Memb. Sci. 363 (2010) 221–231. doi:10.1016/j.memsci.2010.07.032.

[148] V. Mittal, Mechanical and Gas Permeation Properties of Compatibilized Polypropylene – Layered Silicate Nanocomposites, J. Appl. Polym. Sci. 107 (2007) 1350–1361. doi:10.1002/app.

[149] A.J. Monsiváis-Barrón, J. Bonilla-Rios, L.F. Ramos De Valle, E. Palacios, Oxygen permeation properties of HDPE-layered silicate nanocomposites, Polym. Bull. 70 (2013) 939–951. doi:10.1007/s00289-012-0897-5.

[150] C.M.O. Müller, J.B. Laurindo, F. Yamashita, Composites of thermoplastic starch and nanoclays produced by extrusion and thermopressing, Carbohydr. Polym. 89 (2012) 504–510. doi:10.1016/j.carbpol.2012.03.035.

[151] S. NAZARENKO, P. MENEGHETTI, P. JULMON, B. OLSON, S. QUTUBUDDIN, Gas Barrier of Polystyrene Montmorillonite Clay Nanocomposites: Effect of Mineral Layer Aggregation, J. Polym. Sci. Part B Polym. Phys. 45 (2007) 1733–1753. doi:10.1002/polb.

[152] M.A. Osman, J.E.P. Rupp, U.W. Suter, Effect of non-ionic surfactants on the exfoliation and properties of polyethylene-layered silicate nanocomposites, Polymer (Guildf). 46 (2005) 8202–8209. doi:10.1016/j.polymer.2005.06.101.

[153] M.A. Osman, V. Mittal, U.W. Suter, Poly(propylene)-layered silicate nanocomposites: Gas permeation properties and clay exfoliation, Macromol. Chem. Phys. 208 (2007) 68–75. doi:10.1002/macp.200600444.

[154] E. Picard, E. Espuche, R. Fulchiron, Effect of an organo-modified montmorillonite on PLA crystallization and gas barrier properties, Appl. Clay Sci. 53 (2011) 58–65. doi:10.1016/j.clay.2011.04.023.

[155] J. Rhim, S. Hong, H. Park, P. Ng, Preparation and Characterization of Chitosan- Based Nanocomposite Films with Antimicrobial Activity, J. Agric. Food Chem. 54 (2006) 21–23. doi:10.1021/jf060658h.

[156] R.K. Shah, R.K. Krishnaswamy, S. Takahashi, D.R. Paul, Blown films of nanocomposites prepared from low density polyethylene and a sodium ionomer of poly(ethylene-co-methacrylic acid), Polymer (Guildf). 47 (2006) 6187–6201. doi:10.1016/j.polymer.2006.06.051.

[157] A.M. Slavutsky, M.A. Bertuzzi, M. Armada, M.G. García, N.A. Ochoa, Preparation and characterization of montmorillonite/brea gum nanocomposites films, Food Hydrocoll. 35 (2014) 270–278. doi:10.1016/j.foodhyd.2013.06.008.

[158] R. Sothornvit, J.W. Rhim, S.I. Hong, Effect of nano-clay type on the physical and antimicrobial properties of whey protein isolate/clay composite films, J. Food Eng. 91 (2009) 468–473. doi:10.1016/j.jfoodeng.2008.09.026.

[159] R. Sothornvit, S.I. Hong, D.J. An, J.W. Rhim, Effect of clay content on the physical and antimicrobial properties of whey protein isolate/organo-clay composite films, LWT - Food Sci. Technol. 43 (2010) 279–284. doi:10.1016/j.lwt.2009.08.010.

[160] K.E. Strawhecker, E. Manias, Structure and Properties of Poly (vinyl alcohol)/ Na + Montmorillonite Nanocomposites, Chem. Mater. 12 (2000) 2943–2949.

[161] S.K. Swain, S. Dash, C. Behera, S.K. Kisku, L. Behera, Cellulose nanobiocomposites with reinforcement of boron nitride: Study of thermal, oxygen barrier and chemical resistant properties, Carbohydr. Polym. 95 (2013) 728–732. doi:10.1016/j.carbpol.2013.02.080.

[162] M.L. Rodríguez-Marín, L.A. Bello-Pérez, H. Yee-Madeira, Q. Zhong, R.A. González-Soto, Nanocomposites of rice and banana flours blend with montmorillonite: Partial characterization, Mater. Sci. Eng. C. 33 (2013) 3903–3908. doi:10.1016/j.msec.2013.05.027.

[163] X. Tang, S. Alavi, T.J. Herald, Barrier and mechanical properties of starch-clay nanocomposite films, Cereal Chem. 85 (2008) 433–439. doi:10.1094/CCHEM-85-3-0433.

[164] C. Thellen, C. Orroth, D. Froio, D. Ziegler, J. Lucciarini, R. Farrell, et al., Influence of montmorillonite layered silicate on plasticized poly(l-lactide) blown films, Polymer (Guildf). 46 (2005) 11716–11727. doi:10.1016/j.polymer.2005.09.057.

[165] T. Tsai, C. Wen, H. Chuang, M. Lin, U. Ray, Effect of Clay With Different Cation Exchange Capacity on

the Morphology and Properties of Poly (methyl methacrylate)/ Clay Nanocomposites, Polym. Compos. (2009) 1552–1561. doi:10.1002/pc.

[166] T.Y. Tsai, M.J. Lin, C.W. Chang, C.C. Li, Morphology and properties of poly(methyl methacrylate)/clay nanocomposites by in-situ solution polymerization, J. Phys. Chem. Solids. 71 (2010) 590–594. doi:10.1016/j.jpcs.2009.12.044.

[167] J.P.G. Villaluenga, M. Khayet, M.A. López-Manchado, J.L. Valentin, B. Seoane, J.I. Mengual, Gas transport properties of polypropylene/clay composite membranes, Eur. Polym. J. 43 (2007) 1132–1143. doi:10.1016/j.eurpolymj.2007.01.018.

[168] Y.-Q. Wang, Y.-P. Wu, H.-F. Zhang, L.-Q. Zhang, B. Wang, Z.-F. Wang, Free Volume of Montmorillonite/Styrene-Butadiene Rubber Nanocomposites Estimated by Positron Annihilation Lifetime Spectroscopy, Macromol. Rapid Commun. 25 (2004) 1973–1978. doi:10.1002/marc.200400380.

[169] R. Xu, E. Manias, A.J. Snyder, J. Runt, New Biomedical Poly(urethane urea) - Layered Silicate Nanocomposites, Macromolecules. 34 (2001) 337–339.

[170] J.M. Yeh, H.Y. Huang, C.L. Chen, W.F. Su, Y.H. Yu, Siloxane-modified epoxy resin-clay nanocomposite coatings with advanced anticorrosive properties prepared by a solution dispersion approach, Surf. Coatings Technol. 200 (2006) 2753–2763. doi:10.1016/j.surfcoat.2004.11.008.

[171] G. Zehetmeyer, R.M.D. Soares, A. Brandelli, R.S. Mauler, R.V.B. Oliveira, Evaluation of polypropylene/montmorillonite nanocomposites as food packaging material, Polym. Bull. 68 (2012) 2199–2217. doi:10.1007/s00289-012-0722-1.

[172] B. Zhang, Q. Wang, Development of Highly Ordered Nano fi llers in Zein Nanocomposites for Improved Tensile and Barrier Properties, J. Agric. Food Chem. 60 (2012) 4162–4169.

[173] Y. Zhon, D. Janes, Y. Zheng, M. Hetzer, D. De Kee, Mechanical and Oxygen Barrier Properties of Organoclay-Polyethylene Nanocomposite Films Yang, Polym. Eng. Sci. 47 (2007) 1101–1107. doi:10.1002/pen.

[174] A. Fendler, M.P. Villanueva, E. Gimenez, J.M. Lagarón, Characterization of the barrier properties of composites of HDPE and purified cellulose fibers, Cellulose. 14 (2007) 427–438. doi:10.1007/s10570-007-9136-x.

[175] A. Chien, Y. Lee, K. Lin, Crosslinkable Poly (vinyl acetate)/ Clay Nanocomposite Films Cast from Soap-Free Emulsion-Polymerized Latices, J. Appl. Polym. Sci. 109 (2008) 355–362. doi:10.1002/app.

[176] J.M. Herrera-Alonso, E. Marand, J.C. Little, S.S. Cox, Transport properties in polyurethane/clay nanocomposites as barrier materials: Effect of processing conditions, J. Memb. Sci. 337 (2009) 208–214. doi:10.1016/j.memsci.2009.03.045.

[177] Y. Wang, H. Zhang, Y. Wu, J. Yang, L. Zhang, Preparation, structure, and properties of a novel rectorite/styrene-butadiene copolymer nanocomposite, J. Appl. Polym. Sci. 96 (2005) 324–328. doi:10.1002/app.21409.

[178] M.D. Sanchez-Garcia, A. Lopez-Rubio, J.M. Lagaron, Natural micro and nanobiocomposites with enhanced barrier properties and novel functionalities for food biopackaging applications, Trends Food Sci. Technol. 21 (2010) 528–536. doi:10.1016/j.tifs.2010.07.008.

Highlights:

- More than 1000 experimental data of O_2, CO_2 and H_2O permeability are presented

- Impact of nanoparticle shape on permeability is analyzed

- Expected impact of tortuosity on permeability is not systematically achieved

- Selective transport characteristics of nanocomposites is discussed

- Meaningful conclusions on the structure/mass transfer relationship are offered